Nutrient colimitation is a quantitative, dynamic property of microbial populations

Noelle A. Held*
Institute of Biogeochemistry and Pollutant Dynamics, Department of Environmental Systems Science, ETH Zurich, Zurich, Switzerland Department of Environmental Microbiology, Swiss Federal Institute of Aquatic Science and Technology (Eawag), Dübendorf, Switzerland and Department of Biological Sciences, Marine & Environmental Biology Division, University of Southern California, Los Angeles, CA, USA

Aswin Krishna
Department of Biology, ETH Zurich, Zurich Switzerland

Donat Crippa
Department of Environmental Systems Science, ETH Zurich, Zurich, Switzerland

Anastasia Dragan
Institute of Integrative Biology, Department of Environmental Systems Science, ETH Zurich, Zurich, Switzerland

Michael Manhart†
Institute of Integrative Biology, Department of Environmental Systems Science, ETH Zurich, Zurich, Switzerland Department of Environmental Microbiology, Swiss Federal Institute of Aquatic Science and Technology (Eawag), Dübendorf, Switzerland and Center for Advanced Biotechnology and Medicine and Department of Biochemistry and Molecular Biology, Robert Wood Johnson Medical School, Rutgers University, Piscataway, NJ, USA

(Dated: January 8, 2024)

Resource availability dictates how fast and how much microbial populations grow. Quantifying the relationship between microbial growth and resource concentrations makes it possible to promote, inhibit, and predict microbial activity. Microbes require many resources, including macronutrients (e.g., carbon and nitrogen), micronutrients (e.g., metals), and complex resources like vitamins and amino acids. In nature, many of these resources are scarce and their abundances co-vary. This presents the possibility of resource colimitation, when more than one resource limits growth simultaneously. Despite growing evidence for colimitation, the data is difficult to interpret and compare due to lack of quantitative definitions for limitation and colimitation. In this work, we quantify limitation by individual resources using a limitation coefficient and introduce a colimitation index for measuring the effective number of limiting resources. These quantities demonstrate that limitation conditions are not binary or static, but rather exist on a continuum and can change over time as resource conditions change. Furthermore, they allow us to illustrate how limitation of microbial growth rate and biomass yield are related but distinct notions. To demonstrate these concepts, we measure growth of *Escherichia coli* under laboratory conditions, which demonstrates that colimitation is readily accessible in clonal populations under these conditions. Finally, we apply our framework to environmental data to provide intuition for what limitation conditions might exist in nature. Altogether our results provide a quantitative framework for understanding and quantifying colimitation in a wide range of microbial systems.

Keywords: microbial growth, resource limitation, colimitation, growth rate, marine microbes, biogeochemistry, biotechnology, *Escherichia coli*

SIGNIFICANCE STATEMENT

Much of what we know about microbes is from the perspective of a single nutrient limitation, but does this reflect the ecological and evolutionary reality of how microbes live in nature? We present a framework that allows us to assess the extent of nutrient colimitation, providing a quantitative treatment of a problem that is usually interpreted qualitatively. We demonstrate that colimitation of microbial growth rates and biomass yield is relevant in nature and accessible in laboratory conditions, including for clonal populations and independent, elemental resources. This allows us to conclude that the spectrum of microbial growth is best understood in the context of multiple nutrients.

* To whom correspondence should be addressed. Email: nheld@usc.edu
† To whom correspondence should be addressed. Email: mmanhart@rutgers.edu

INTRODUCTION

Resource availability controls the growth, physiology, and activity of microbes. Microbes need many resources to grow, and in nature many of these resources are simultaneously rare [1–3]. A basic concept for modeling microbial growth in the context of multiple resources is Liebig's Law of the Minimum, which states that growth is determined by availability of the scarcest resource relative to biological demand. While Liebig's law was originally defined for agricultural plant yields, the idea has since been applied to other systems such as the growth of animals [4, 5], human populations [6], and microbes [7], the latter being the focus of this study.

Liebig's law of the minimum has largely defined experimentation and modeling of microbial growth in resource limitation. Ecosystem and biogeochemical models that incorporate resource limitation of microbial growth rates and biomass production often employ a minimizing function [8–11]. In laboratory experiments, it is customary to designate a specific limiting resource, while keeping other resources in excess. This approach has demonstrated that the growth, physiology, and molecular biology of microorganisms are influenced by the identity of the limiting resource [12–16]. However, focusing on single, binary resource limitations restricts our understanding and predictions of microbial growth in nature, where microbes experience a continuous range of resource concentrations and where many resources are simultaneously scarce [17–22].

There are hints that microbial growth could be, and in nature often is, simultaneously limited by multiple resources (resource colimitation). One line of evidence comes from biogeochemistry. In systems such as the open ocean, the elemental composition of the environment reflects that of abundant microbes suggesting a balance between supply and biological demand [1, 22, 23]. Accordingly, in situ factorial experiments in which resources are supplemented individually and in combinations sometimes find super-additive effects of adding multiple resources [2, 19, 21, 24–27]. Resource colimitation has also been explored in laboratory experiments in which microbial populations drew down multiple resources simultaneously [28, 29]. Finally, in microbial communities, ecological theory predicts the coexistence of multiple species within a resource supply range, with each species depleting a specific resource, leading to colimitation of the community as a whole [30–33].

Though resource colimitation has been acknowledged since the earliest literature [34], a central question remains: Is resource colimitation an exception, or a rule? So far, interpretations have been limited by lack of a common quantitative framework. Many models have been proposed, and are usually phenomenological in nature. The variety of discrete models used in different studies means that the current literature lacks the ability to quantitatively assess resource colimitation as opposed to single resource, Liebig-type limitation [18, 20, 35].

In this study, we quantitatively describe the phenomenon of resource-limited microbial growth including when growth depends on multiple resources simultaneously (colimitation). For illustration, we focus on the basic case of colimitation by biologically necessary, non-substitutable, independent resources such as carbon (C) and nitrogen (N), as opposed to when resources are substitutable or when there is a direct biochemical dependence (i.e., uptake of one resource is dependent on the other). To build a fundamental understanding of the phenomenon of resource colimitation, we concentrate on clonal populations rather than microbial communities. We introduce metrics that precisely quantify the extent of limitation and colimitation in a microbial population; these metrics highlight the continuous and dynamic nature of resource limitation, in contrast to the binary and static interpretations of limitation used in many previous studies. In particular, we quantify colimitation by an effective number of limiting resources, which measures how many resources affect growth in a particular ecological state. We first apply these concepts to laboratory measurements of *Escherichia coli* growth on glucose and ammonium, which shows that colimitation conditions for these resources are readily accessible, rather than requiring a precise fine-tuning of parameters. We then demonstrate the applicability of our framework to data for a wide range of microbial species in natural environments. Altogether our results provide a general framework for understanding and quantifying resource colimitation in microbes.

RESULTS

Growth rate limitation is a quantitative, dynamic property of a microbial population. The growth rate of a microbial population depends on the concentrations of resources, such as carbon or nitrogen sources, in the environment. The best-known model of how growth rate $g(R)$ depends on a resource concentration R is the Monod model [36, 37] (Fig. 1A):

$$g(R) = g_{\max}\frac{R}{R+K}, \tag{1}$$

where $g_{\max}$ is the maximum growth rate when the resource concentration is infinite, and K is the half-saturation resource concentration at which growth rate is half $g_{\max}$. Although the approach of this paper is applicable to any growth model, we will focus on the Monod model since it is the most commonly-used and has been used to describe a wide of range of data.

The continuous dependence of growth rate on resource concentration, as exemplified by the Monod model, indicates that we should think of resource limitation as also being a quantitative property of populations and their resources, rather than as a binary state of limiting or

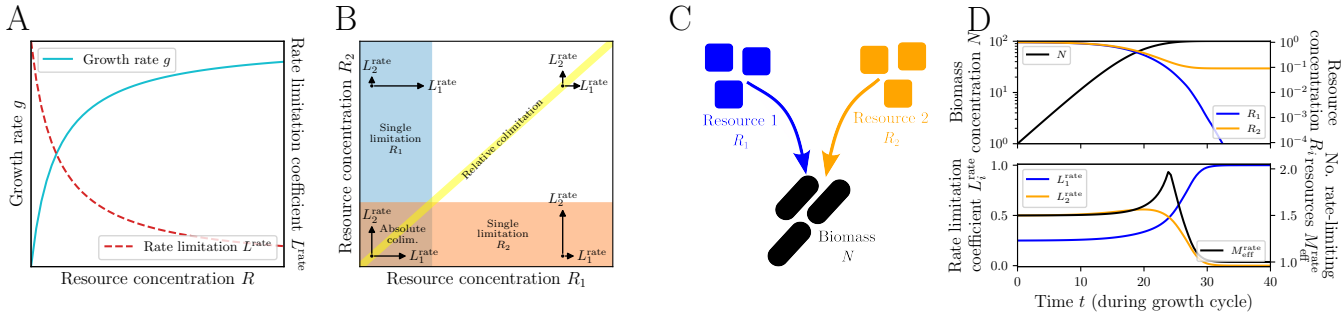

FIG. 1. **Resource limitation and colimitation of population growth rate.** (A) Schematic of growth rate $g(R)$ (solid cyan line) as a function of environmental resource concentration R. This is representative of the typical Monod-like dependence (Eq. 1) we assume in this article, as has been empirically measured [36, 37]. We also show the growth rate limitation coefficient $L^{\rm rate}(R)$ (dashed red line; Eq. 2) across the same resource concentrations. (B) Schematic of concentration space for two resources, showing different limitation conditions. The black arrows show limitation coefficients $L_i^{\rm rate}$ for each resource at different combinations of concentrations, and the shaded regions mark regions of high limitation for resource 1 (blue) and resource 2 (orange). The yellow diagonal band marks the approximate region of relative colimitation, where the number of limiting resources $M_{\rm eff}^{\rm rate}$ is close to 2. (C) Diagram for a model of biomass with concentration N consuming two resources with concentrations R_1 (blue) and R_2 (orange). (D) Simulation of batch culture dynamics for the model in (C). The top panel shows the growth of biomass (black line) as the two resources (blue and orange) are depleted over time. The bottom panel shows the limitation coefficients $L_i^{\rm rate}$ and the number of limiting resources $M_{\rm eff}^{\rm rate}$ over the same time range.

non-limiting. We therefore define the growth rate limitation coefficient for this resource as the relative change in growth rate for a small relative change in resource concentration [29, 38] (Fig. 1A):

$$L^{\rm rate} = \frac{R}{g}\frac{\partial g}{\partial R}. \tag{2}$$

This quantity is defined in analogy with control coefficients in metabolic control analysis [39]. For most growth rate models (including the Monod model), the limitation coefficient ranges from $L^{\rm rate} = 0$ at infinite resource concentrations to $L^{\rm rate} = 1$ at zero concentrations (Supplementary Information Sec. S1). In particular, $L^{\rm rate} = K/(R+K)$ for the Monod model with a single resource (Eq. 1, Fig. 1A).

Multiple resources can be absolutely or relatively colimiting. Models of a single resource such as the Monod model may not fully describe microbial growth, which relies on multiple resources including sources of carbon, nitrogen, phosphorus, and trace metals. We can thus define a limitation coefficient $L_i^{\rm rate}$ for each resource i using Eq. 2, where the growth rate depends on M resources $g(R_1, R_2, \ldots, R_M)$. This raises the possibility of *colimitation*, in which multiple resources can be simultaneously limiting growth. Determining which and how many resources affect growth is important because the growth, physiology, and molecular properties of cells are dependent on the identity of the limiting resource(s), not just the degree of limitation [12]. Additionally, the growth response to a pulse or fluctuation in resources will depend both on the nature of the limitation and degree of limitation [40].

We distinguish between two types of colimitation. *Absolute colimitation* between two resources i and j occurs when their limitation coefficients $L_i^{\rm rate}$ and $L_j^{\rm rate}$ are simultaneously large (Fig. 1B). *Relative colimitation* between two resources occurs when their limitation coefficients are similar, regardless of their absolute magnitudes. We introduce a quantitative index for relative colimitation, defined as the sum of limitation coefficients for all resources normalized by the largest limitation coefficient:

$$M_{\rm eff}^{\rm rate} = \frac{\sum_{{\rm resource}\ i} L_i^{\rm rate}}{\max_{{\rm resource}\ i} L_i^{\rm rate}}. \tag{3}$$

It has a minimum value of $M_{\rm eff}^{\rm rate} = 1$ if only one resource has nonzero limitation coefficient, and a maximum value of $M_{\rm eff}^{\rm rate} = M$ (the total number of resources) if all resources have equal limitation. Therefore we can interpret $M_{\rm eff}^{\rm rate}$ as the effective number of resources that relatively colimit growth rate. This quantity is maximized along a diagonal region (yellow area in Fig. 1B) in the space of resource concentrations, where both resources are equally limiting. Note that this overlaps the region of absolute colimitation, but also extends to conditions where both resources are not limiting in absolute terms but still have similar relative limitation.

For example, consider a population consuming two essential resources, shown schematically in Fig. 1C. Figure 1D (top panel) shows the dynamics of the biomass and resource concentrations in a batch culture (Methods). The biomass concentration increases exponentially while the two resources are depleted. While the orange resource is at first more limiting, it is the blue resource that runs out first (bottom panel of Fig. 1D). At the point where the limitation coefficients cross over each other, the effective number of limiting resources $M_{\rm eff}^{\rm rate}$ equals

exactly 2, since both resource are equally limiting. In Fig. S1 we show analogous scenarios for continuous cultures (chemostat), where resources are supplied to the population at constant rate (Supplementary Information Secs. S2 and S3).

Growth rate colimitation is readily accessible under laboratory conditions. To realize these colimitation conditions in the laboratory, we varied glucose and ammonium over ranges of concentrations and measured the growth rates of a clonal population of *Escherichia coli* under these conditions (Figs. 2A, S5, and Fig. S6; Methods; Dataset S1). We fit the data to several models of growth rate dependence $g(R_1, R_2, \ldots, R_M)$ on multiple resources, since previous work has not established a consensus on which one is most accurate or whether they describe biologically different scenarios [5, 18, 29, 35, 41, 42]. We focus especially on four of the most common models (Fig. S2, first row; Methods and Supplementary Information Sec. S4): the Liebig model (also known as Blackman rate limitation or the "law of the minimum") [18, 29, 41], the Poisson arrival time (PAT) model [5, 41], the additive model (also known as the Bloomfield model) [5, 41], and the multiplicative model [5, 29, 35]. All four models share the same key properties: growth rate is zero if any resource is zero (all resources are essential [43], also sometimes called heterologous [29], non-interactive [44], or complementary [45] resources); they reduce to the Monod model for a single resource (Eq. 1) if all other resources are unlimited; and they saturate at a finite maximum growth rate $g_{\max}$ when all resources are unlimited (Supplementary Information Sec. S4).

While the dependence of growth rate on resource concentration appears similar across these models (Fig. S2, first row), the models differ when we consider their limitation properties (Fig. S2, second and third rows). In particular, the models show a gradient of colimitation: the Liebig model has no colimitation by construction, whereas the multiplicative model has colimitation over the widest range of resource concentrations, with the PAT and additive models in between (Fig. S2 and Fig. S3). While here we focus on essential, non-substitutable resources like carbon and nitrogen sources, we can also extend this analysis to pairs of resources that are substitutable [43] (e.g., different carbon sources, also known as Type II colimitation [18] or homologous resources [29]; Supplementary Information Sec. S5 and Fig. S4) or chemically-dependent (or Type III colimitation [18]; Supplementary Information Sec. S6 and Fig. S4).

We fit each of the four growth rate models to this data (Fig. S7). Of these four models, the Liebig minimizing model performed worst in describing the data, while all three non-Liebig models performed better. Although the quality of fit was similar among the non-Liebig models, we found a slight preference for the multiplicative model. Another model allowing for Hill coefficients matched the data even better, but at the cost of additional parameters (Supplementary Information Sec. S4). We used this best-fit multiplicative model to calculate the limitation and colimitation regimes in Fig. 2B,C. This shows significant colimitation by glucose and ammonium ($M_{\text{eff}}^{\text{rate}} > 1$). The region of high colimitation overlaps with the estimated range of resource concentrations experienced by *E. coli* in nature (Fig. 2C; Methods; Dataset S2).

Quantifying growth rate colimitation across species and resources in natural environments. We have shown that colimitation can occur in the laboratory, but is it also realized in nature? To demonstrate this, we collected measurements of half-saturation resource concentrations K_i (measured from the dependence of growth rate on that resource concentration according to the Monod model [37]) and environmental concentrations R_i for those same resources across many organisms (Fig. 3A, Methods, Dataset S2).

We use this data to estimate limitation for each resource, assuming all other resources for these organisms are present at very high concentrations. Since the true dependence of growth rate on multiple resources is unknown for these organisms and resources, we test all four growth rate models from Fig. S2 to calculate limitation coefficients in Fig. 3B. We find significant limitation coefficients for many of the marine species, but low limitation for the freshwater and enteric species. This is evident from the R and K data itself; most half-saturation concentrations K are less than their corresponding environmental concentrations R, which means low limitation, with the exceptions being several marine strains on phosphate and nitrate (Fig. 3A). Next we quantify relative colimitation between these resources using the number of limiting resources $M_{\text{eff}}^{\text{rate}}$ (Fig. 3C). While several of the marine species show high colimitation, we also see intermediate levels of colimitation for some enteric species, even though their absolute levels of limitation are low (Fig. 3B).

Dynamics of resource depletion. Besides affecting *how fast* a population grows (growth rate), resource concentrations also determine *how much* new biomass grows over a period of time (biomass yield). In Fig. 4A, consider a batch culture where resources are supplied as one initial pulse and then are depleted until growth stops (for an analogous case in chemostat cultures, see Fig. S8). The shape of these trajectories is dictated by the instantaneous resource efficiency Y_i of each resource i (Methods and Supplementary Information Sec. S8); this is the amount of new biomass produced per unit of that resource, at a given set of resource concentrations. If the efficiencies do not depend on resource concentrations, then these trajectories are straight lines (Fig. 4A, green line; Supplementary Information Sec. S8) and the slope is the ratio of instantaneous efficiencies for the two resources (Supplementary Information Sec. S8). On the other hand, if the resource efficiencies vary over the growth cycle — for example, because they depend on the external resource concentrations which change over time — then the resource depletion trajectories can curve

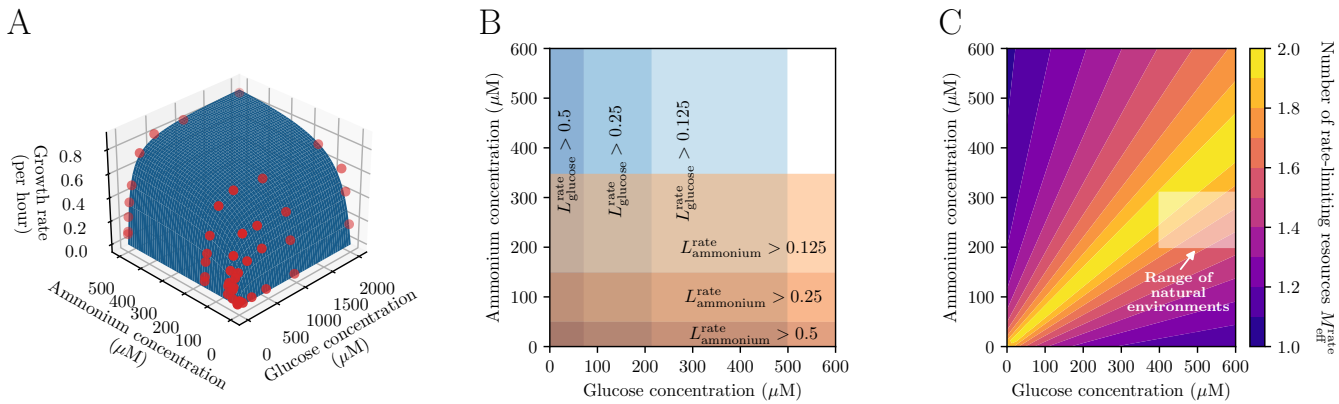

FIG. 2. **Experimental measurement of growth rate limitation and colimitation.** (A) Growth rate measurements (red points) over glucose and ammonium concentrations for *E. coli* in minimal medium (Methods, Dataset S1; see Figs. S5 and S6 for growth curves). The blue surface is the best-fit model (multiplicative model; Methods and Fig. S7; $g_{\max} \approx 1.0$ hour^{-1}, $K_{\text{glucose}} \approx 71$ μM, $K_{\text{ammonium}} \approx 50$ μM). (B) Using the model fitted in (A), we calculate regions of growth rate limitation coefficients L^{rate} (Eq. 2) for glucose (blue) and ammonium (orange) across concentrations. The overlap between these regions indicates conditions where both resources are absolutely colimiting (compare to Fig. 1B). (C) Using the model fitted in (A), we calculate growth rate colimitation of glucose and ammonium (number of limiting resources $M^{\text{rate}}_{\text{eff}}$, Eq. 3) across concentrations of both resources. The white box indicates the approximate range of glucose and ammonium concentrations found in natural environments for *E. coli* (Methods, Dataset S2).

(Fig. 4A, orange line; see also Fig. S9). Possible mechanisms for dynamic resource efficiency include resource consumption to maintain existing biomass (Supplementary Information Sec. S9) and growth rate-regulated proteome allocation (Supplementary Information Sec. S10).

Many models assume that biomass growth only stops when one or more resources reach zero concentration (vertical and horizontal gray dashed lines in Fig. 4A, with resource trajectories stopping at the green and orange squares). However, in practice biomass growth may stop at some nonzero resource concentrations (curved gray dashed line in Fig. 4A, with resource trajectories stopping at the green and orange crosses), often denoted by R^* [30]. It is possible for resource thresholds to depend on each other, for instance in the presence of a constant death or dilution rate (Supplementary Information Sec. S8; see also Fig. S10).

Biomass yield limitation is quantified by the response to a perturbation in resource supply. How do we define limitation of biomass yield? Intuitively, we could consider which resource reaches zero concentration by the end of growth (i.e., which axis the depletion trajectory hits first in Fig. 4A) [28]. However, this chemical definition masks the fact that resource limitation is a biological phenomenon. The chemical definition may also be impractical, because it is often not possible to empirically determine if a resource is completely exhausted in an environment, and because growth may stop before this point.

Alternatively, we can measure the response of biomass production to a perturbation in the resource supply and define limitation from the biological response. This approach is commonly used in field studies in the aquatic sciences [1, 18, 21, 22, 46]. Figure 4B illustrates a typical scenario for this: we start with a population in a state of zero growth rate, supplement each resource i by some amount ΔR_i, and measure how much biomass grows after a growth cycle. In Fig. 4B, we see that supplementing resource 1 (dashed blue arrow) leads to no additional biomass (inset, blue bar), while supplementing resource 2 (dashed red arrow) leads to significant additional biomass (inset, red bar); we could interpret this as showing that resource 2 is limiting biomass production. To detect colimitation, we can supplement both resources together (Fig. 4B, dashed purple arrow) and see how much additional biomass grows; in this example, the same amount of biomass grows with the double supplement compared to supplementing resource 2 alone, suggesting the biomass yield is only under single limitation for resource 2.

This factorial approach can be difficult to interpret when the starting condition of the experiment is concealed [20]. This is because the outcome clearly depends on the amounts of each resource that we choose to supplement. Figure 4C shows a similar supplementation experiment, but where the amounts of added resources are greater than in Fig. 4B. In this case, adding resource 1 alone has no effect, but adding it in combination with resource 2 produces a greater amount of biomass than adding resource 2 alone. The reason is that the perturbation has switched the identity of the resource that gets ultimately exhausted; this is sometimes referred to as serial limitation. The problem is evident even in this simple Liebig-minimizing case, and would be exacerbated in situations in which colimitation is occurring (Fig. S11).

One way to constrain resource colimitation without

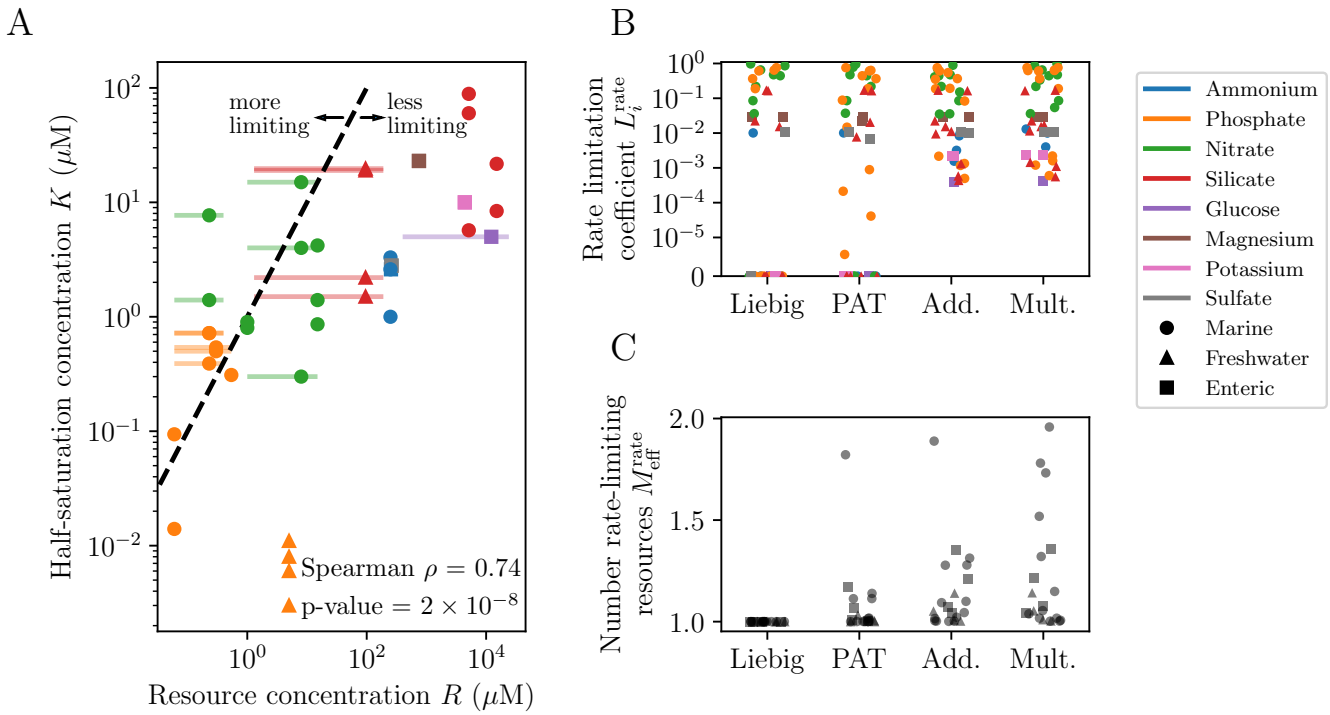

FIG. 3. **Applying growth rate limitation concepts to empirical data across species and resources.** (A) Representative half-saturation concentrations K (μM) versus environmental concentrations R (μM) for data from various organisms, resources, and environments collected from the literature (Dataset S2). When we found environmental concentrations R as ranges, we indicate this by horizontal bars in the plot. Scatter points are colored based on the resource being considered; marker shape indicates the habitat. The Spearman correlation coefficient between R and K is $\rho \approx 0.74$ with a p-value $\approx 2 \times 10^{-8}$. (B) Rate limitation coefficients (L_i^{rate}) calculated from the data shown in (A); we calculated limitation coefficients for individual resources in all organism/resource combinations, considering different growth rate models (horizontal axis: Liebig = Liebig model, PAT = Poisson arrival time model, Add. = additive model, Mult. = multiplicative Monod model; Methods, Supplementary Information Sec. S4). (C) Number of rate-limiting resources $M_{\text{eff}}^{\text{rate}}$ calculated from the data shown in (A), also considering the same growth rate models as in (B). Each organism has data for a pair of resources, such that the maximum number of limiting resources is 2.

prior knowledge of the starting state is to scan a surface of supplementation amounts, rather than focusing on a single factorial supplementation [20]. For instance, in Fig. 4D we start with a population that has zero concentration of both resources, and then we supplement both resources in different amounts and measure the total biomass after a growth cycle. The data is then visualized as a heatmap of added biomass yield (Fig. 4E), rather than a set of bars for each discrete condition (Fig. 4B,C, insets).

The systematic scan of resource surfaces allows a quantitative definition of limitation to be applied and interpreted without prior knowledge of the system's starting conditions. We define realized biomass yield limitation for a resource as the relative change in biomass for a relative change in the added resource:

$$L^{\text{yield}} = \frac{R}{N}\frac{\partial N}{\partial R}. \tag{4}$$

We also quantify relative colimitation in terms of the effective number of yield-limiting resources:

$$M_{\text{eff}}^{\text{yield}} = \frac{\sum_{\text{resource } i} L_i^{\text{yield}}}{\max_{\text{resource } i} L_i^{\text{yield}}}. \tag{5}$$

Biomass yield limitation is not equivalent to growth rate limitation. Mathematically, the limitation metrics for growth rate (Eqs. 2 and 3) and biomass yield (Eqs. 4 and 5) are similar. However, they are biologically distinct: the former describes the effect on how *fast* growth occurs, while the latter describes the effect on how *much* growth occurs. Growth rate limitation is an instantaneous property of a population. In contrast, biomass yield limitation is a property of a population realized over a finite time period. A population can experience multiple different growth rate limitation regimes over that time period, and these may or many not match the limitation for biomass yield over the whole time.

The distinction between growth rate and biomass yield is analogous to properties of cars. The maximum speed of a car may be limited by air intake or drag, while the range will be limited by fuel or battery capacity. These

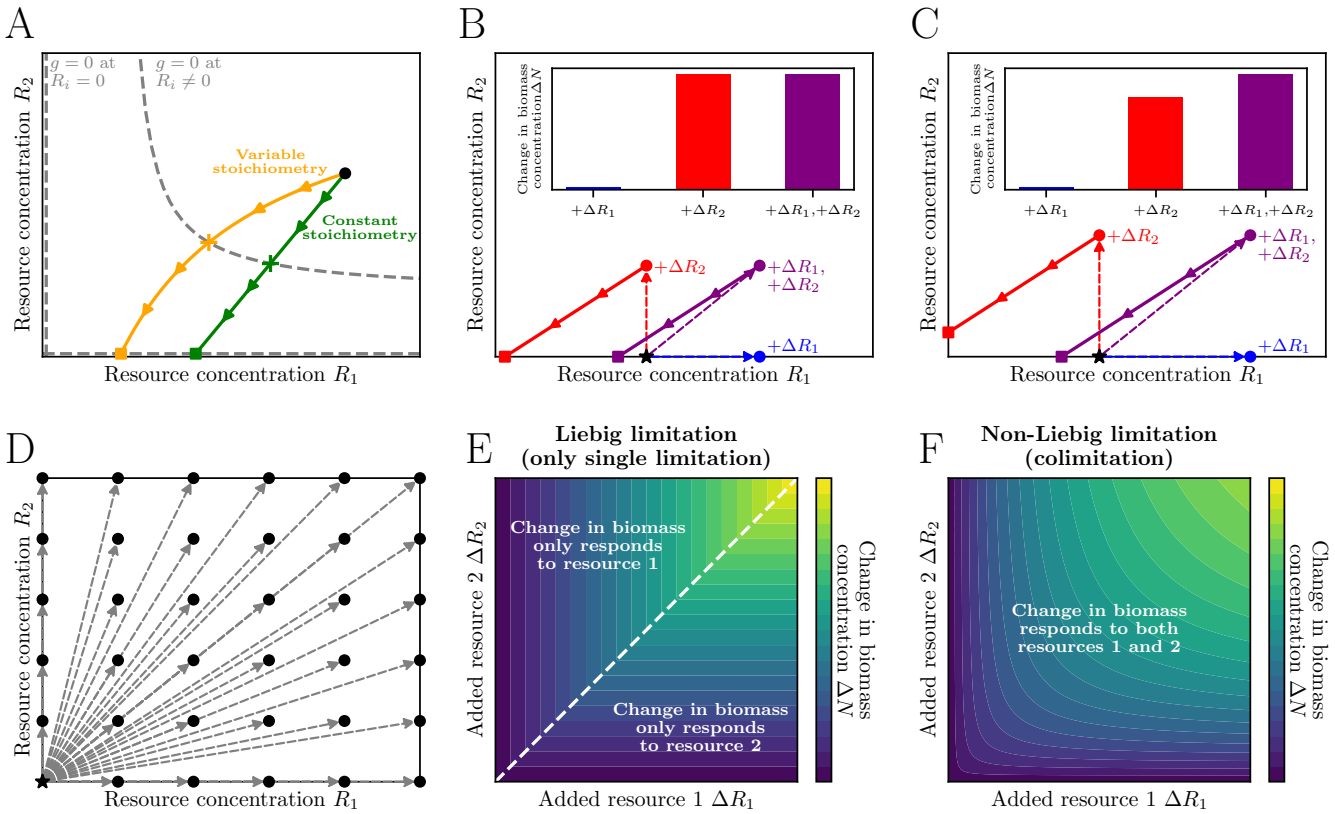

FIG. 4. **Depletion dynamics of resources and concepts of yield limitation and colimitation.** (A) Schematic depletion dynamics for two resources over a batch culture growth cycle. The trajectory of resource concentrations under constant stoichiometry (green line with arrows) must be straight (Supplementary Information Sec. S8), while the trajectory can curve (orange line with arrows) if stoichiometry is variable. Squares mark potential endpoints of the trajectories if growth only stops when at least one resource is completed depleted (vertical and horizontal gray dashed lines), and crosses mark potential endpoints if growth stops at a nonzero combination of resource concentrations (curved gray dashed line). (B) Schematic of a resource supplementation experiment in the space of two resource concentrations. The biomass starts at the black star where it is no longer growing (due to depletion of resource 2). We then supplement either resource 1 (dashed blue line), resource 2 (dashed red line), or both (dashed purple line). The resource depletion trajectories that follow are shown as solid lines with arrows, starting from the dots and ending at the squares. In the inset, we show the amount of additional biomass ΔN produced along each of these trajectories, with colors matching the different supplementations. (See Fig. S11 for an example with a non-Liebig model.) (C) Same as (B) but with larger amounts of supplemented resources. (D) Schematic of a systematic scan of resource supplements, where we start from a population depleted for both resources (at the black star) and systematically add many different combinations of both resources (dashed gray lines). We then track biomass growth starting from each black star and plot how that new biomass amount varies with the amounts of the supplemented resources. (E) Example of biomass production as a function of two supplemented resources, resulting from the setup in (D). The white dashed lines partitions supplementation conditions into a set of conditions where the change in biomass only responds to supplementing one resource or the other, but not both. This is therefore an example of Liebig limitation for biomass (Eq. 6, Supplementary Information Sec. S8). (F) Same as (E) but with non-Liebig biomass limitation, where biomass production depends on both supplemented resources simultaneously.

variables might interact, but are largely independent of each other. Which of these limitation properties is more important to a system depends on the context. For microbes, growth rate limitation is likely to be more important to evolution, since growth rate is under direct selection while biomass production may not be (depending on spatial structure and privatization of resources [47]). Biomass yield limitation, on the other hand, may be important in situations where we care about environmental and ecological composition, like elemental cycling in the ocean or total production in biotechnology applications [48–50].

Biomass yield colimitation arises from interactions between resources. The classic way to model biomass yield is Liebig's law; note that Liebig's law for biomass yield is biologically distinct from that of growth rate, although it is conceptually similar. As in the case of growth rate, only one resource at a time can have a nonzero limitation coefficient L^{yield} for yield, and thus the number of yield-limiting resources is always

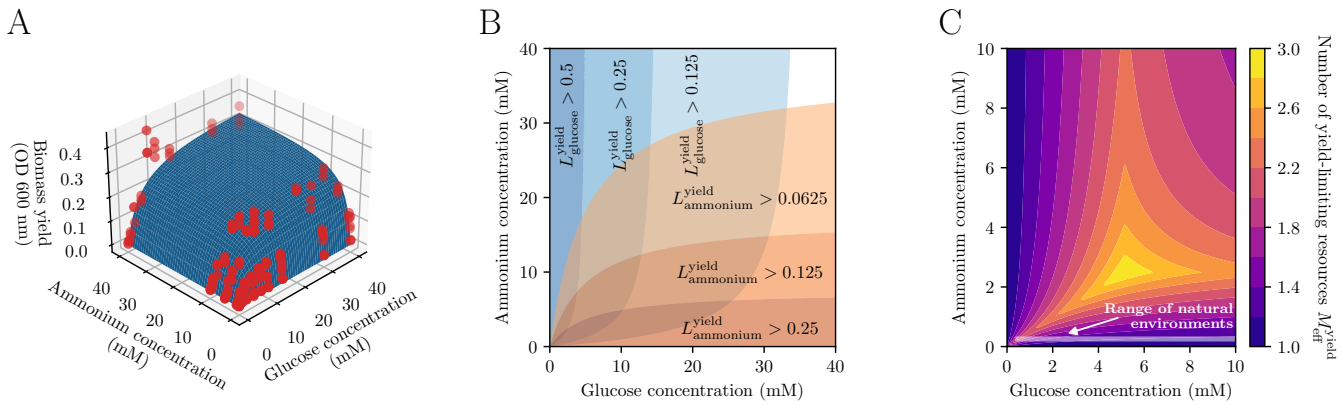

FIG. 5. **Experimental measurements of yield limitation and colimitation.** (A) Biomass measurements (as optical density at 600 nm, red points) over glucose and ammonium concentrations for *E. coli* in minimal medium (Methods, Dataset S3; see Figs. S13 and S14 for growth curves). The blue surface is the best-fit model (generalized-mean model with $N_{\text{fixed}} \approx 0.39$ OD, $Y_{\text{glucose}} \approx 0.076$ OD/mM glucose, $Y_{\text{ammonium}} \approx 0.16$ OD/mM ammonium, $q \approx -1.0$, Eq. 7; Methods and Supplementary Information Sec. S12). (B) Using the model fitted in (A), we calculate regions of yield limitation coefficients L^{yield} (Eq. 4) for glucose (blue) and ammonium (orange) across concentrations. The overlap between these regions indicates conditions where both resources are absolutely colimiting. (C) Using the model fitted in (A), we calculate yield colimitation of glucose and ammonium (number of yield-limiting resources $M^{\text{yield}}_{\text{eff}}$, Eq. 5) across concentrations of both resources. Note that the apparent maximum number of limiting resources is $M^{\text{yield}}_{\text{eff}} = 3$ because of the third, unmeasured resource that becomes limiting for biomass yield when glucose and ammonium are saturated.

$M^{\text{yield}}_{\text{eff}} = 1$. The biomass yield is set by whichever resource is stoichiometrically scarcest (Fig. 4E and Supplementary Information Sec. S8):

$$N = \min_{\text{resource } i} R_i Y_i, \tag{6}$$

where N is the amount of biomass that can be produced, R_i is the resource concentration, and Y_i is the resource efficiency of the population growing on that resource.

Alternatively, we can consider a non-Liebig case, where biomass responds to small changes in both resources simultaneously (Fig. 4F). In this case, all resources have nonzero yield limitation coefficients L^{yield}_i, and therefore there is nonzero yield colimitation ($M^{\text{yield}}_{\text{eff}} > 1$). This implies that there are interactions between the resources. Briefly, if the biomass yield on one resource depends on the other resource, or if the concentration of one resource at which growth stops depends on the other resource, then biomass production will depend on both resources simultaneously, and hence the two resources will be colimiting. For further discussion, see Supplementary Information Sec. S8.

Biomass yield colimitation is readily accessible under laboratory conditions. As with growth rate, we can determine conditions under which two resources colimit biomass yield by systematically varying them and measuring biomass production under laboratory conditions (Figs. S13 and S14). We take as an example *E. coli* growing in batch conditions with varying initial supply of a carbon source (glucose) and a nitrogen source (ammonium). Figure 5A shows how the total biomass of *E. coli* in batch conditions varies with the initial supply of glucose and ammonium. To determine yield limitation at these different concentrations, we fit this dependence to a model. We use a phenomenological model of biomass N dependence on resources R_i inspired by the mathematical concept of a generalized mean (Supplementary Information Sec. S12, Fig. S12):

$$N(R_1, R_2, \ldots, R_M) = \left(\sum_{\text{resource } i} (R_i Y_i)^q \right)^{1/q}, \tag{7}$$

where Y_i is the resource efficiency (biomass produced per unit of resource i). We interpret the parameter q as quantifying the extent of interaction between resources. In the limit of $q \to -\infty$, this model is equivalent to the Liebig model (Eq. 6; Fig. S12). Finite values of q therefore represent deviations from the Liebig model, implying an interaction between the resources (Supplementary Information Sec. S8). For this reason, we call q the interaction parameter. Finite values of q mean there is some range of conditions where resources colimit biomass yield (Fig. S12). We fit this model to our data and it matches closely (Fig. 5A), with a finite q value and a statistically significant improvement over the Liebig model (Fig. S15).

As with growth rate, we can now use the fitted model to quantify biomass yield limitation and colimitation (Fig. 5B,C). Unmeasured resources will eventually limit biomass once the focal resources are sufficiently abundant. We model this as limitation by a third, hidden resource; however, in practice a non-nutrient constraint such as production of a toxin or limitation for physical

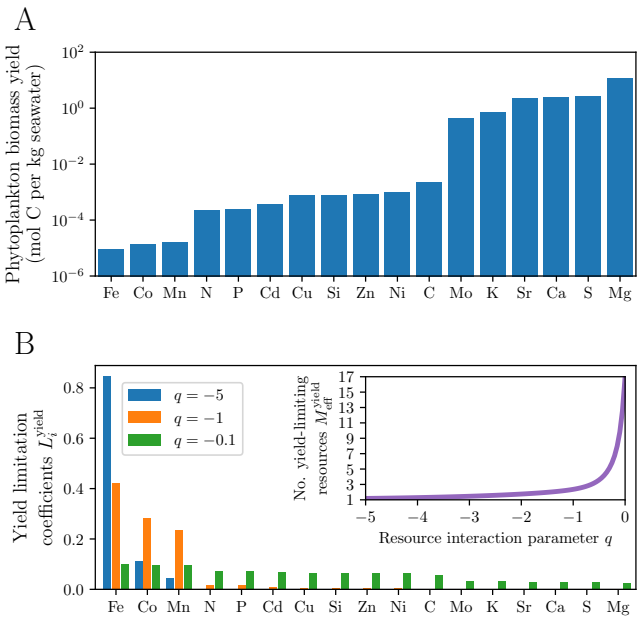

FIG. 6. **Applying yield limitation concepts to empirical data for marine phytoplankton.** (A) Estimated phytoplankton biomass yield per kg of seawater supported by each elemental resource's environmental concentration. Data is from Moore et al. [1] (Supplementary Table S1 therein). (B) Using biomass yields from (A), we calculate yield limitation coefficients L^{yield} for each elemental resource. Since we do not know the underlying model for how multiple resources contribute to biomass, we calculate limitation using different values of the resource interaction parameter q (colors) in the generalized-mean model of biomass (Eq. 7, Supplementary Information Sec. S12). Inset: Number of yield-limiting resources $M_{\text{eff}}^{\text{yield}}$ as a function of the interaction parameter q, using data from (A).

space could also occur. Thus, there is a condition where the model predicts three limiting resources. For *E. coli*, biomass yield colimitation is evident in environmentally relevant concentrations (Fig. 5C), suggesting that in nature, *E. coli* biomass production is best understood in the context of multiple resources.

Estimating biomass yield limitation and colimitation in natural environments. We have demonstrated that a microbial population can be yield-limited for multiple resources under laboratory conditions, but how likely is such colimitation in nature? We consider elemental resources for phytoplankton in the ocean, using coarse-grained data from Moore et al. [1]. Using the measured elemental composition of phytoplankton, we calculate the biomass yield for the available concentration of each element (Fig. 6A). This shows roughly three tiers of resources, separated by orders of magnitude: the trace metals iron, cobalt, and manganese have the lowest yields, followed by another set of similar yields for nitrogen, phosphorus, and other metals. The remaining elements all have much higher yields.

We calculate yield limitation coefficients for each resource using the resource concentrations and resource efficiencies (as ratios relative to carbon) reported by Moore et al. [1]. Since we do not know how biomass depends on multiple resources, we use the generalized-mean model (Eq. 7) to make predictions for representative values of the interaction parameter q (Fig. 6B). For lower values of q (less interaction), limitation is more strongly concentrated in the resource most rare relative to their biomass requirements, especially iron. This is because this regime is closer to Liebig limitation, where only one resource (the most rare) can be limiting at a time. For higher values of q, we see more equal levels of limitation across resources. The inset of Fig. 6B quantifies this using the number of yield limiting resources $M_{\text{eff}}^{\text{yield}}$.

Given that the macronutrients N and P are known to be limiting to marine phytoplankton, it is interesting that N and P limitation are only appreciably limiting in the strong interaction scenarios. While the data we used is coarse-grained and does not account for temporal, spatial, and biological variability (including plasticity in resource use), it does capture overall patterns in resource availability in the surface ocean [1]. The results imply that to determine the true level of colimitation for these populations, we would need to measure the dependence of phytoplankton biomass across many resources simultaneously.

DISCUSSION

The importance of resource colimitation. Multiple lines of evidence point to the importance of resource colimitation in determining microbial growth, activity (including biochemical rates), and physiology. The most mature examples are in the aquatic sciences, mainly marine but also to a lesser extent in freshwater systems. Most of what is known is from combinatorial resource addition experiments, where resources are predicted to be limiting from biogeochemical data and are added individually and in combinations to microbial communities sampled in situ [20]. These experiments have collectively demonstrated that resource colimitation is a relatively common state in ocean ecosystems [2, 18]. However, the great majority of this data is focused on primary production/photosynthetic organisms [19, 51], and also tends to focus on colimitation between dependent resources, such as a trace metal required for uptake of a macronutrient [18]. Thus, it is not clear whether resource colimitation is a common across organisms, environmental contexts, and outside of specific biochemical dependencies.

Because most evidence for resource colimitation comes from in situ experiments, the theory of resource colimitation is best developed for microbial communities, as opposed to clonal populations or individual organisms. The idea is that different members of the community have different resource preferences and biomass stoichiometries, such that different organisms are limited for different resources resulting in a community-level colimita-

tion [33]. The effect may be exacerbated by metabolic dependencies between organisms [32]. At the same time, systems biologists have also predicted the possibility of resource colimitation in laboratory systems. The concept has been in the literature since the 1970s, notably in work by Droop [52] and by Valdkamp and Jannasch [53], who pointed out that laboratory experiments that provide artificially high concentrations of resources besides a focal limiting resource do not reflect the realities of nature. Modern metabolic models also predict the possibility of resource colimitation, particularly when variable stoichiometry, either in terms of absolute elemental stoichiometry or stoichiometry of resource allocation, is considered [35, 54]. While variable stoichiometry is thought to be most common in autotrophic organisms such as phytoplankton, it has also been observed and linked to resource colimitation in heterotrophic consumers [20].

The fact that we find evidence of colimitation for two essential, independent resources in the model organism *E. coli*, and in particular in resource concentrations that are relevant to *E. coli*'s natural environments, highlights a need for closer attention to resource colimitation in a wider variety of systems. Prior studies have also investigated resource colimitation of *E. coli*, but used a chemical definition, i.e., whether multiple resources were simultaneously depleted [28, 55, 56]. In contrast, we suggest a biological definition (how is growth affected by the resources?) because 1) this allows precise identification of resource colimitation for different growth, activity, or physiological parameters of interest; 2) this strategy can be used in either batch or chemostat cultures, meaning also that growth rate and growth yield colimitation can be quantified separately (see S3) ; and 3) this allows instantaneous definitions of resource limitation and colimitation. It is important to note that our example occurs in a clonal population of heterotrophic bacteria. In other settings, such as an in situ experiment from a complete microbial community, community-level colimitation would be layered on this backdrop.

Mechanisms of colimitation. Intuitively, resource colimitation implies interactions among resources that limit microbial growth. The most clear examples include biochemically-dependent resource colimitation and substitutable resource colimitation, and our framework can be extended to these scenarios. In independent resource colimitation, such a tradeoff could still occur due to constraints on molecular composition, resource uptake, and energy utilization that is exacerbated when multiple resources are rare. This could manifest in fine-scale molecular networks and/or as stoichiometric flexibility, which could be a direct result of growth optimization in resource colimited conditions [35, 54]. Additionally, we cannot rule out the role of phenotypic heterogeneity [57] driving a population-level response. This would be relevant if a subset of the population is primarily limited for one resource while another subset is limited for another resource [33].

There are also environmental drivers. In aquatic systems with low resource concentrations, microscale environmental heterogeneity can reduce the chance that cells encounter both necessary resources quickly; this is implicit in the Poisson Arrival Time (PAT) model that we have considered. A combination of micro- and macroscale biogeochemical cycling implies that resources covary in predictable ways; organisms could take advantage of this and regulate their growth in response to multiple resources. In a broad sense, ecological and biogeochemical theory indicates that the requirements of microbial life and the elemental composition of their surroundings coevolve with one another. This may increase the possibility for resource colimitation in nature [58, 59].

Inferring resource colimitation in nature. A challenge in the existing literature on resource colimitation is the difficulty in assessing the results of combinatorial resource addition experiments [20]. The trouble is that the starting resource conditions are usually unknown (and are indeed inferred from the results of the experiment), and the results are highly dependent on the ratio and concentration of resources added. This can lead to inadvertent serial colimitation, which can be resolved but hinders interpretation of the biological endpoint of the experiment (i.e., if omics or physiological data is taken at the end of the incubation). These experiments are also limited to binary interpretations of limitation and colimitation and cannot resolve the spectrum of biological responses. Supplementation experiments that scan a surface of resource concentrations in multiple dimensions would in this case provide a critical advantage for quantifying the extent of limitation and the number of limiting resources. However, this would require a high-throughput addition experiment, and would be challenging in many in situ contexts with traditional methods.

Another approach is to use molecular biomarkers of limitation and colimitation to measure in situ resource status. At least for single resource limitation, this is already occurring in marine biogeochemistry and human microbiome contexts [2, 60, 61]. These biomarkers could be validated and calibrated in the laboratory, then quantified in natural samples. The biomarker approach has the benefit of being able to avoid experimental effects in laboratory or in situ perturbations, and to identify how strain and even sub-strain level resource limitations vary in the community [62]. If resource colimitation represents a distinct physiological state for a population or community, it is possible that specific biomarkers for resource colimitation can also be identified. Our quantitative definitions L^{rate}, L^{yield}, $M_{\text{eff}}^{\text{rate}}$, and $M_{\text{eff}}^{\text{yield}}$ would allow direct, quantitative comparisons between experiments and in situ resource conditions, bridging the gap between the lab and nature and making a truly quantitative biomarker calibration possible.

Rate limitation vs yield limitation. Our results highlight that there is a fundamental difference between growth rate limitation and biomass yield limitation. Previous work has also referred to these as "kinetic" and "stoichiometric" limitations [29]. Specifically, it is possi-

ble for two different resources or sets of resources to be limiting for rate versus yield. It is important to distinguish between rate and yield limitation depending on the context. For instance, a study about the rate of a biogeochemical process may be more concerned with rate limitation, whereas a study about long-term ecological stoichiometry may be more concerned with yield. In either of these cases, it is not necessarily possible to infer the limiting resource(s) for rate by establishing the limiting resource(s) for yield, and vice versa. In evolutionary contexts, this is relevant because selection depends on the physical context, with growth rate being selected for in well-mixed scenarios and yield being selected for in spatially structured scenarios.

There is a body of literature describing rate-yield tradeoffs that occur due to fundamental constraints on cellular resource allocation [63]. While this trade off is theoretically predicted, there has been limited empirical evidence in many systems [64, 65]. Distinct resource limiting rate versus yield will not cause these tradeoffs in the first place (since yields evolve neutrally in the absence of spatial structure [47]), but an existing tradeoff could maintain distinct resources limiting rate and yield.

Growth limitation beyond resource concentrations. Resource availability is not the only control on microbial growth, particularly in nature. Limited availability of physical resources such as light and space can limit population growth [66–68]. In the ocean, predators and viral lysis kill a substantial number of cells per day and have quantitative effects on growth rates and standing stocks of microbes [69, 70]. In host-associated microbiomes, such as the human gut, viral lysis also plays a role, as does the host immune system [71, 72]. In all of these contexts, there is also the possibility of intermicrobial warfare such as toxin release, as well as the opposite, promotion of growth through quorum-sensing behaviors due to the presence of other bacteria [73, 74]. There is still much to learn about how these factors interact with resource limitations to influence microbial growth. While the dependence of growth on these other factors is likely more complex than it is on resource availability (e.g., non-monotonic dependence), it is possible to extend the limitation metrics we present here to these cases as well, such that one can consider multiple factors at once (e.g., resource availability and virus concentrations).

x Resource colimitation of microbial populations and communities may be a common state of nature, instead of a special case. It is a sensible outcome of eco-evolutionary theory and biogeochemistry and has been observed in natural habitats ranging from the surface ocean to the human microbiome. As we have shown, careful experimental design, including testing for colimitation across 2D resource ranges, enhances the opportunity to observe colimitation and identify colimitation conditions for further experimentation. Quantitative metrics of limitation and colimitation, as we have introduced here, will facilitate laboratory measurements of the underlying biochemical, molecular, physiological, and ecological mechanisms. This is important because as examples in *E. coli* and in nature have shown, colimitation is possible and even likely in the natural resource conditions in which organisms evolve. This context is critical for understanding even the most fundamental properties of cells, can help us to better predict, manage, and exploit the growth of microbes, and underscores the connectivity between microbial life and the composition of the environment.

METHODS

Numerical methods. We performed all numerical calculations in Python version 3.10.9, using tools from NumPy [75] version 1.24.1 and SciPy [76] version 1.10.0. We prepared all figures using Matplotlib [77] version 3.7.1.

Model of batch growth. Throughout the main text we focus on microbial growth under batch conditions, meaning an initial biomass is given a fixed supply of resources, which it consumes until growth stops. Let $N(t)$ be the concentration of biomass and $\mathbf{R}(t) = (R_1(t), R_2(t), \ldots, R_M(t))$ the vector of all M resource concentrations in the environment at time t, with some fixed initial conditions $N(0)$ and $\mathbf{R}(0)$. Their dynamics over time are determined by

$$\begin{aligned} \frac{d}{dt}N(t) &= g(\mathbf{R}(t))N(t), \\ \frac{d}{dt}R_i(t) &= -\frac{1}{Y_i}\frac{d}{dt}N(t), \end{aligned} \tag{8}$$

where $g(\mathbf{R})$ is the per-capita biomass growth rate that depends on the environmental resource concentrations and Y_i is the intrinsic yield (amount of new biomass produced per unit resource, with all other resource unlimited) for resource i. We solve these equations numerically using `scipy.integrate.solve_ivp` (e.g., Fig. 1D).

Summary of growth rate models. We focus on four widely-used models of how growth rate depends on multiple resources. In the case of two resources, these models are

$$
\begin{aligned}
\text{Liebig model [18, 29, 41]: } g(R_1,R_2) &= \min\left(\frac{g_{\max,1}R_1}{R_1+K_1}, \frac{g_{\max,2}R_2}{R_2+K_2}\right),\\
\text{Poisson arrival time (PAT) model [5, 41]: } g(R_1,R_2) &= g_{\max}\frac{\frac{R_1}{K_1}\frac{R_2}{K_2}\left(\frac{R_1}{K_1}+\frac{R_2}{K_2}\right)}{\frac{R_1}{K_1}\frac{R_2}{K_2}\left(\frac{R_1}{K_1}+\frac{R_2}{K_2}\right)+\left(\frac{R_1}{K_1}\right)^2+\frac{R_1}{K_1}\frac{R_2}{K_2}+\left(\frac{R_2}{K_2}\right)^2},\\
\text{Additive model [5, 41]: } g(R_1,R_2) &= g_{\max}\frac{\frac{R_1}{K_1}\frac{R_2}{K_2}}{\frac{R_1}{K_1}\frac{R_2}{K_2}+\frac{R_1}{K_1}+\frac{R_2}{K_2}},\\
\text{Multiplicative model [5, 29]: } g(R_1,R_2) &= g_{\max}\left(\frac{R_1}{R_1+K_1}\right)\left(\frac{R_2}{R_2+K_2}\right),
\end{aligned}
\tag{9}
$$

where $g_{\max}$ is the maximum possible growth rate and K_i is the half-saturation concentration for resource i. Supplementary Information Sec. S4 contains complete details of these models, including generalizations of these models to an arbitrary number of resources and some heuristic derivations.

Experimental measurement of bacterial growth curves. To profile the growth of bacteria in nutrient colimitation, we used the strain *Escherichia coli* sp. MG1655 pCS-λ [78], which contains a luciferase protein expressed from the constitutive Lambda CS promoter under kanamycin selection. We selected single clones and grew overnight cultures in modified M9 minimal medium. This medium base was composed of a modified M9 salt base without nitrogen (for 1 L of 5X concentrated M9 salt base without nitrogen: 64 g $Na_2HPO_4 \cdot 7H_2O$ (Sigma Aldrich BioXtra grade lot SLBV4967, CAS S9390-500G), 15 g KH_2PO_4 monobasic (Sigma Aldrich ACS grade lot SZBF350AV CAS P0062-500G), and 2.5 g NaCl (Sigma Aldrich BioXtra grade lot SYBG1530V CAS S7653-250G)). We also added 500 mM $MgSO_4$ hexahydrate (Sigma Aldrich ACS grade Lot BCBT5460) and 50 μg/mL kanamycin (Sigma Aldrich CAS 70560-51-9 Lot 0000130025). For overnight cultures, we added 20 mM ammonium chloride (Sigma Aldrich ACS Reagent Lot STBH3180 CAS 31107-500G) and 10 mM D(+)glucose (Sigma Aldrich BioXtra grade Lot SLBW5196 CAS G7528-1Kg); previous experiments indicated that this combination provides for nutrient replete growth with ultimate biomass yield limitation by glucose.

After growing into stationary phase overnight, we collected the cells by centrifugation and washed three times in the modified 1X M9 salts without nitrogen, then adjusted to OD 0.01 in the modified 1X M9 salts without nitrogen. We inoculated the cells in a 1:100 ratio resulting in a final OD of 0.0001 into the wells of white walled, flat base 96 well plates (Corning) containing the 1X modified M9 medium without nitrogen and pre-defined combinations of ammonium chloride and D-glucose, which were added from concentrated stocks prepared in the 1X modified M9 salt without nitrogen base. For the scan of growth rate, we varied ammonium between 0 and 1 mM and glucose between 0 and 2 mM. We monitored luminescence across triplicate plates, measured simultaneously using three plate readers from the same manufacturer (Biotek Synergy H1) with similar settings implemented (37 C, orbital shaking of 15 s prior to each measurement, luminescence integration time of 3 s). For the scan of biomass yield, we varied ammonium between 0 and 40 mM and glucose between 0 and 150 mM. In that case we monitored growth as optical density at 600 nm using the Tecan Infinite F200 spectrophotometer, connected to the Tecan Evo 200 automated liquid handling system and the Liconic STX100 integrated, automated incubator. Raw growth curve data is in Datasets S1 and S3.

Analysis of growth curve data for growth rates and biomass yield. We analyzed growth curves using the open source AMiGA library [79]. In the growth rate data, we observed an initial spike in luminescence at the immediate start of the experiment due to acclimation or possible condensation, so we truncated the first six data points prior to AMiGA fitting. We did not use any truncation for the biomass yield data from OD. We then performed a background correction by subtracting the T=0 timepoint from all OD/luminescence values. We verified growth properties fitted by AMiGA by visually comparing them to the growth curves (Figs. S5, S6, S14, and S14). The fitted growth rates and yields are in Datasets S1 and S3.

We then fit growth rates and biomass yields to models using `scipy.optimize.curve_fit` for least-squares minimization, which reports optimal parameter values and their estimated standard deviations. For the yield scans with replicate measurements, we also estimated uncertainties on fits by bootstrapping 100 simulating data sets from these parameters. We did this by randomly sampling (with replacement) three yields from the three replicate measurements at each initial glucose and ammonium concentration combination. We calculated the Akaike information criterion (corrected for small sample size) for each model fit using

$$
\mathrm{AIC} = 2n + n\log\left(\frac{\sum_{i=1}^{n}(f_i-y_i)^2}{n-k}\right) - 2k\left(\frac{k+1}{n-k-1}\right), \tag{10}
$$

where n is the number of data points, y_i is the ith measured data point, f_i is the fitted value for that data point, and k is the number of parameters in the model [80]. We calculate the relative Akaike weight for a model α as

$$w_\alpha = \frac{e^{-\frac{1}{2}\mathrm{AIC}_\alpha}}{\sum_{\mathrm{model}\,\beta} e^{-\frac{1}{2}\mathrm{AIC}_\beta}}. \tag{11}$$

Data collection for growth response traits and environmental resource concentrations. We collected 20 studies in which the parameters of the Monod growth model ($g_{\max}$ and K) for two resoures were measured for the same species/strain. We extracted this data from a broader literature review of Monod parameters that we conducted earlier [37]. Whenever possible, we estimated background environmental nutrient concentrations (i.e., the concentrations the organism is expected to experience in the environment from which it was isolated) from data provided in the original manuscript. When this was not provided, we estimated a range of environmental concentrations from the expected habitat of the organism. For instance, for *E. coli* sp. K12, we selected representative environmental concentrations of resources in the human gut (higher concentrations) and in soils (lower concentrations). For marine diatoms, we selected representative environmental concentrations of high nutrient regions (coastal upwelling zones) and low nutrient regions (surface open ocean). In some cases, the expected resource concentration range is large and spans at least an order of magnitude. For calculations, the midpoint of this range was used. Using the measured Monod parameters and estimated environmental concentrations, we calculated limitation coefficients using four common models (Liebig, poisson arrival time model, additive model, and multiplicative model).

SUPPLEMENTARY INFORMATION

Supplementary figures S1-S15 can be found at the end of this document. Supplementary discussion and associated references can be found in the SI Appendix. Experimental and literature-derived data used in this study can be found in Datasets S1-S3.

AUTHOR CONTRIBUTIONS

NAH and MM conceived and designed the study. NAH, AK, and MM developed the conceptual framework and analyzed models. NAH, AK, DC, and AD performed laboratory experiments. NAH and MM wrote and edited the manuscript with contributions from all authors.

CONFLICTS OF INTEREST

The authors declare no conflict of interest.

ACKNOWLEDGEMENTS

We thank Daniel Angst for help running the automated growth curve measurements and Justus Fink for valuable feedback on this paper. NAH was supported by the Principles of Microbial Ecosystems collaboration of the Simons Foundation (grant ID 542379 to Martin Ackermann) and an ETH Zurich Career Seed Grant (SEED-26 21-2 to NAH). MM was supported by an Ambizione grant from the Swiss National Science Foundation (PZ00P3_180147).

[1] C. M. Moore, M. M. Mills, K. R. Arrigo, I. Berman-Frank, L. Bopp, P. W. Boyd, E. D. Galbraith, R. J. Geider, C. Guieu, S. L. Jaccard, T. D. Jickells, J. La Roche, T. M. Lenton, N. M. Mahowald, E. Marañón, I. Marinov, J. K. Moore, T. Nakatsuka, A. Oschlies, M. A. Saito, T. F. Thingstad, A. Tsuda, and O. Ulloa. Processes and Patterns of Oceanic Nutrient Limitation. *Nat Geoscience*, 6:701–710, 2013.

[2] Thomas J. Browning and C. Mark Moore. Global analysis of ocean phytoplankton nutrient limitation reveals high prevalence of co-limitation. *Nature Communications*, 14(1):5014, August 2023.

[3] Enzai Du, César Terrer, Adam F. A. Pellegrini, Anders Ahlström, Caspar J. van Lissa, Xia Zhao, Nan Xia, Xinhui Wu, and Robert B. Jackson. Global patterns of terrestrial nitrogen and phosphorus limitation. *Nat Geosci*, 13:221–226, 2020.

[4] James J. Elser, Dean R. Dobberfuhl, Neil A. MacKay, and John H. Schampel. Organism Size, Life History, and N:P Stoichiometry: Toward a unified view of cellular and ecosystem processes. *BioScience*, 46(9):674–684, October 1996.

[5] E. Sperfeld, D. Martin-Creuzburg, and A. Wacker. Multiple resource limitation theory applied to herbivorous consumers: Liebig's minimum rule vs. interactive co-limitation. *Ecol Lett*, 15:142–150, 2012.

[6] Joel E. Cohen. Population Growth and Earth's Human Carrying Capacity. https://www.science.org/doi/10.1126/science.7618100, 1995.

[7] H.J.W. De Baar. Von Liebig's law of the minimum and plankton ecology (1899–1991). *Progress in Oceanography*, 33(4):347–386, January 1994.

[8] Emily J. Zakem and Naomi M. Levine. Systematic Variation in Marine Dissolved Organic Matter Stoichiometry and Remineralization Ratios as a Function of Lability. *Global Biogeochemical Cycles*, 33(11):1389–1407, 2019.

[9] Michael J Follows, Stephanie Dutkiewicz, Scott Grant, and Sallie W Chisholm. Emergent biogeography of microbial communities in a model ocean. *Science (New York, N.Y.)*, 315(5820):1843–6, March 2007.

[10] Michael J Follows and Stephanie Dutkiewicz. Modeling diverse communities of marine microbes. *Annual review of marine science*, 3:427–451, 2011.

[11] Nicolas Gruber, Charles D. Keeling, and Nicholas R. Bates. Interannual Variability in the North Atlantic Ocean Carbon Sink. *Science*, 298(5602):2374–2378, 2002.

[12] Sophia Hsin-Jung Li, Zhiyuan Li, Junyoung O. Park, Christopher G. King, Joshua D. Rabinowitz, Ned S. Wingreen, and Zemer Gitai. Escherichia coli translation strategies differ across carbon, nitrogen and phosphorus limitation conditions. *Nature Microbiology*, 3(8):939–947, August 2018.

[13] Prasad Gyaneshwar, Oleg Paliy, Jon McAuliffe, David L. Popham, Michael I. Jordan, and Sydney Kustu. Sulfur and Nitrogen Limitation in Escherichia coli K-12: Specific Homeostatic Responses. *Journal of Bacteriology*, 187(3):1074–1090, February 2005.

[14] Larry Reitzer. Nitrogen assimilation and global regulation in Escherichia coli. *Annual Review of Microbiology*, 57:155–176, 2003.

[15] Daniel R. Brown, Geraint Barton, Zhensheng Pan, Martin Buck, and Sivaramesh Wigneshweraraj. Nitrogen stress response and stringent response are coupled in Escherichia coli. *Nature Communications*, 5(May):1–8, 2014.

[16] Daniel P. Zimmer, Eric Soupene, Haidy L. Lee, Volker F. Wendisch, Arkady B. Khodursky, Brian J. Peter, Robert A. Bender, and Sydney Kustu. Nitrogen regulatory protein C-controlled genes of Escherichia coli: Scavenging as a defense against nitrogen limitation. *Proceedings of the National Academy of Sciences*, 97(26):14674–14679, December 2000.

[17] M. Danger, C. Oumarou, D. Benest, and G. Lacroix. Bacteria can control stoichiometry and nutrient limitation of phytoplankton. *Functional Ecology*, 21(2):202–210, 2007.

[18] M. A. Saito, T. J. Goepfert, and J. T. Ritt. Some thoughts on the concept of colimitation: Three definitions and the importance of bioavailability. *Limnol Oceanogr*, 53:276–290, 2008.

[19] W. Stanley Harpole, Jacqueline T. Ngai, Elsa E. Cleland, Eric W. Seabloom, Elizabeth T. Borer, Matthew E.S. Bracken, James J. Elser, Daniel S. Gruner, Helmut Hillebrand, Jonathan B. Shurin, and Jennifer E. Smith. Nutrient co-limitation of primary producer communities. *Ecology Letters*, 14(9):852–862, 2011.

[20] Erik Sperfeld, David Raubenheimer, and Alexander Wacker. Bridging factorial and gradient concepts of resource co-limitation: Towards a general framework applied to consumers. *Ecology Letters*, 19(2):201–215, 2016.

[21] Thomas J Browning, P Eric, Insa Rapp, Anja Engel, Erin M Bertrand, Alessandro Tagliabue, and C Mark Moore. Nutrient co-limitation at the boundary of an oceanic gyre. *Nature Publishing Group*, 12, 2017.

[22] James J. Elser, Matthew E.S. Bracken, Elsa E. Cleland, Daniel S. Gruner, W. Stanley Harpole, Helmut Hillebrand, Jacqueline T. Ngai, Eric W. Seabloom, Jonathan B. Shurin, and Jennifer E. Smith. Global analysis of nitrogen and phosphorus limitation of primary producers in freshwater, marine and terrestrial ecosystems. *Ecology Letters*, 10(12):1135–1142, 2007.

[23] Kevin R Arrigo. Marine microorganisms and global nutrient cycles. *Nature*, 437(September):349–356, 2005.

[24] Thomas J. Browning, Eric P. Achterberg, Anja Engel, and Edward Mawji. Manganese co-limitation of phytoplankton growth and major nutrient drawdown in the Southern Ocean. *Nature Communications*, 12(1):884, February 2021.

[25] Benjamin S. Twining, Sara Rauschenberg, Steven E. Baer, Michael W. Lomas, Adam C. Martiny, and Olga Antipova. A nutrient limitation mosaic in the eastern tropical Indian Ocean. *Deep Sea Research Part II: Topical Studies in Oceanography*, 166:125–140, August 2019.

[26] Erin M. Bertrand, Mak a. Saito, Julie M. Rose, Christina R. Riesselman, Maeve C. Lohan, Abigail E. Noble, Peter a. Lee, and Giacomo R. DiTullio. Vitamin B12 and iron colimitation of phytoplankton growth in the Ross Sea. *Limnology and Oceanography*, 52(3):1079–1093, 2007.

[27] J. Keith Moore and Scott C. Doney. Iron availability limits the ocean nitrogen inventory stabilizing feedbacks between marine denitrification and nitrogen fixation. *Global Biogeochemical Cycles*, 21(2):1–12, 2007.

[28] Thomas Egli and Manfred Zinn. The concept of multiple-nutrient-limited growth of microorganisms and its application in biotechnological processes. *Biotechnology Advances*, 22(1-2):35–43, 2003.

[29] M. Zinn, B. Witholt, and T. Egli. Dual nutrient limited growth: Models, experimental observations, and applications. *J Biotechnol*, 113:263–279, 2004.

[30] D. Tilman. Tests of Resource Competition Theory Using Four Species of Lake Michigan Algae. *Ecology*, 62(3):802–815, 1981.

[31] David Tilman. THE RESOURCE-RATIO HYPOTHESIS OF PLANT SUCCESSION. *The American Naturalist*, 125(6):827–852, 1985.

[32] Catherine Bannon, Insa Rapp, and Erin M. Bertrand. Community Interaction Co-limitation: Nutrient Limitation in a Marine Microbial Community Context. *Frontiers in Microbiology*, 13, 2022.

[33] Michael Danger, Tanguy Daufresne, Françoise Lucas, Serge Pissard, and Gérard Lacroix. Does Liebig's law of the minimum scale up from species to communities? *Oikos*, 117(11):1741–1751, 2008.

[34] M.R. Droop. Some thoughts on nutrient limitation in algae. *J. Phycol*, 9:264–272, 1974.

[35] Kai W. Wirtz and Onur Kerimoglu. Autotrophic Stoichiometry Emerging from Optimality and Variable Colimitation. *Frontiers in Ecology and Evolution*, 4, 2016.

[36] J. Monod. The growth of bacterial cultures. *Annu Rev Microbiol*, 3:371–394, 1949.

[37] J. W. Fink, N. A. Held, and M. Manhart. Microbial population dynamics decouple growth response from environmental nutrient concentration. *Proc Natl Acad Sci USA*, 120:e2207295120, 2023.

[38] M. Rutgers, P. A. Balk, and K. van Dam. Quantification of multiple-substrate controlled growth-simultaneous ammonium and glucose limitation in chemostat cultures of Klebsiella pneumoniae. *Arch Microbiol*, 153:478–484, 1990.

[39] R. Heinrich and S. Schuster. *The Regulation of Cellular Systems*. Chapman and Hall, New York, 1996.

[40] Jen Nguyen, Juanita Lara-Gutiérrez, and Roman Stocker. Environmental fluctuations and their effects on microbial communities, populations and individuals. *FEMS Microbiology Reviews*, 45(4):fuaa068, July 2021.

[41] R. V. O'Neill, D. L. DeAngelis, J. J. Pastor, B. J. Jackson, and W. M. Post. Multiple nutrient limitations in ecological models. *Ecol Modelling*, 46:147–163, 1989.

[42] J.-C. Poggiale, M. Baklouti, B. Queguiner, and S. A. L. M. Kooijman. How far details are important in ecosystem modelling: The case of multi-limiting nutrients in phytoplankton–zooplankton interactions. *Phil Trans R Soc B*, 365:3495–3507, 2010.

[43] D. Tilman. Resources: A graphical-mechanistic approach to competition and predation. *Am Nat*, 116:362–393, 1980.

[44] F. G. Bader. Analysis of double-substrate limited growth. *Biotechnol Bioeng*, 20:183–202, 1978.

[45] B. C. Baltzis and A. G. Fredrickson. Limitation of growth rate by two complementary nutrients: Some elementary but neglected considerations. *Biotechnol Bioeng*, 31:75–86, 1988.

[46] Daniel R. O'Donnell, Paul Wilburn, Eugene A. Silow, Lev Y. Yampolsky, and Elena Litchman. Nitrogen and phosphorus colimitation of phytoplankton in Lake Baikal: Insights from a spatial survey and nutrient enrichment experiments. *Limnology and Oceanography*, 62(4):1383–1392, 2017.

[47] H. Bachmann, M. Fischlechner, R. N. Barfa, F. Branco dos Santos, D. Molenaar, and B. Teusink. Availability of public goods shapes the evolution of competing metabolic strategies. *Proc Natl Acad Sci USA*, 110:14302–14307, 2013.

[48] Paul A. del Giorgio and Jonathan J. Cole. Bacterial Growth Efficiency in Natural Aquatic Systems. *Annual Review of Ecology and Systematics*, 29(1):503–541, 1998.

[49] Casey M. Godwin, Emily A. Whitaker, and James B. Cotner. Growth rate and resource imbalance interactively control biomass stoichiometry and elemental quotas of aquatic bacteria. *Ecology*, 98(3):820–829, 2017.

[50] David A. Lipson. The complex relationship between microbial growth rate and yield and its implications for ecosystem processes. *Frontiers in Microbiology*, 6, 2015.

[51] M. E. S. Bracken, H. Hillebrand, E. T. Borer, E. W. Seabloom, J. Cebrian, E. E. Cleland, J. J. Elser, D. S. Gruner, W. S. Harpole, J. T. Ngai, and J. E. Smith. Signatures of nutrient limitation and co-limitation: responses of autotroph internal nutrient concentrations to nitrogen and phosphorus additions. *Oikos*, 124:113–121, 2015.

[52] M.R. Droop. Some thoughts on nutrient limitation in algae. *J Phycol*, 9:264–272, 1974.

[53] H. Veldkamp and Holger W. Jannasch. Mixed culture studies with the chemostat. *J Appl Chem Biotechnol*, 22:105–123, 1972.

[54] S. Sharma and R. Steuer. Modelling microbial communities using biochemical resource allocation analysis. *J R Soc Interface*, 16:20190474, 2019.

[55] Thomas Egli. On multiple-nutrient-limited growth of microorganisms, with special reference to dual limitation by carbon and nitrogen substrates. *Antonie van Leeuwenhoek*, 60:225–234, 1991.

[56] Karin Kovárová-Kovar and Thomas Egli. Growth Kinetics of Suspended Microbial Cells: From Single-Substrate-Controlled Growth to Mixed-Substrate Kinetics. *Microbiol Mol Biol Rev*, 62:646–666, 1998.

[57] Frank Schreiber, Sten Littmann, Gaute Lavik, Stéphane Escrig, Anders Meibom, Marcel M.M. Kuypers, and Martin Ackermann. Phenotypic heterogeneity driven by nutrient limitation promotes growth in fluctuating environments. *Nature Microbiology*, 1(6):1–7, 2016.

[58] Megan L. Larsen, Steven W. Wilhelm, and Jay T. Lennon. Nutrient stoichiometry shapes microbial coevolution. *Ecology Letters*, 22(6):1009–1018, 2019.

[59] François M. M. Morel. The co-evolution of phytoplankton and trace element cycles in the oceans. *Geobiology*, 6(3):318–324, 2008.

[60] Mak A Saito, Matthew R McIlvin, Dawn M Moran, Tyler J Goepfert, Giacomo R. DiTullio, Anton F. Post, and Carl H Lamborg. Multiple nutrient stresses at intersecting Pacific Ocean biomes detected by protein biomarkers. *Science*, 345:1173–7, 2014.

[61] Xianfeng Zeng, Xi Xing, Meera Gupta, Felix C. Keber, Jaime G. Lopez, Ying-Chiang J. Lee, Asael Roichman, Lin Wang, Michael D. Neinast, Mohamed S. Donia, Martin Wühr, Cholsoon Jang, and Joshua D. Rabinowitz. Gut bacterial nutrient preferences quantified in vivo. *Cell*, 185:3441–3456.e19, 2022.

[62] Natalie R. Cohen, Matthew R. McIlvin, Dawn M. Moran, Noelle A. Held, Jaclyn K. Saunders, Nicholas J. Hawco, Michael Brosnahan, Giacomo R. DiTullio, Carl Lamborg, John P. McCrow, Chris L. Dupont, Andrew E. Allen, and Mak A. Saito. Dinoflagellates alter their carbon and nutrient metabolic strategies across environmental gradients in the central Pacific Ocean. *Nature Microbiology*, 2021.

[63] T. Pfeiffer and S. Bonhoeffer. Evolution of cross-feeding in microbial populations. *Am Nat*, 163:E126–E135, 2004.

[64] M. Novak, T. Pfeiffer, R. E. Lenski, U. Sauer, and S. Bonhoeffer. Experimental tests for an evolutionary tradeoff between growth rate and yield in E. coli. *Am Nat*, 168:242–251, 2006.

[65] C. Cheng, E. J. O'Brien, D. McCloskey, J. UtrillaI, C. Olson, R. A. LaCroix, T. E. Sandberg, A. M. Feist, B. O. Palsson, and Z. A. King. Laboratory evolution reveals a two-dimensional rate-yield tradeoff in microbial metabolism. *PLoS Comput Biol*, 15:e1007066, 2019.

[66] Hugh Venables and C. Mark Moore. Phytoplankton and light limitation in the Southern Ocean: Learning from high-nutrient, high-chlorophyll areas. *J Geophys Res: Oceans*, 115:C02015, 2010.

[67] Katharine Z. Coyte, Hervé Tabuteau, Eamonn A. Gaffney, Kevin R. Foster, and William M. Durham. Microbial competition in porous environments can select against rapid biofilm growth. *Proc Natl Acad Sci USA*, 114:E161–E170, 2017.

[68] Diarmuid P. Lloyd and Rosalind J. Allen. Competition for space during bacterial colonization of a surface. *J R Soc Interface*, 12:20150608, 2015.

[69] Yi-Chun Yeh and Jed A. Fuhrman. Effects of phytoplankton, viral communities, and warming on free-living and particle-associated marine prokaryotic community structure. *Nat Commun*, 13:7905, 2022.

[70] Curtis A Suttle. Marine viruses — major players in the global ecosystem. *Nat Rev Microbiol*, 5:801–812, 2007.

[71] Danping Zheng, Timur Liwinski, and Eran Elinav. Interaction between microbiota and immunity in health and disease. *Cell Rese*, 30:492–506, 2020.

[72] Zhirui Cao, Naoki Sugimura, Elke Burgermeister, Matthias P. Ebert, Tao Zuo, and Ping Lan. The gut virome: A new microbiome component in health and disease. *eBioMedicine*, 81:104113, 2022.

[73] Elisa T. Granato, Thomas A. Meiller-Legrand, and Kevin R. Foster. The Evolution and Ecology of Bacterial Warfare. *Curr Biol*, 29:R521–R537, 2019.

[74] Steven T. Rutherford and Bonnie L. Bassler. Bacterial Quorum Sensing: Its Role in Virulence and Possibilities for Its Control. *Cold Spring Harb Perspect Med*, 2:a012427, 2012.

[75] C. R. Harris, K. J. Millman, S. J. van der Walt, R. Gommers, P. Virtanen, D. Cournapeau, E. Wieser, J. Taylor, S. Berg, N. J. Smith, R. Kern, M. Picus, S. Hoyer, M. H. van Kerkwijk, M. Brett, A. Haldane, J. Fernández del Río, M. Wiebe, P. Peterson, P. Gérard-Marchant, K. Sheppard, T. Reddy, W. Weckesser, H. Abbasi, C. Gohlke, and T. E. Oliphant. Array programming with NumPy. *Nature*, 585:357–362, 2020.

[76] P. Virtanen, R. Gommers, T. E. Oliphant, M. Haberland, T. Reddy, D. Cournapeau, E. Burovski, P. Peterson, W. Weckesser, J. Bright, S. J. van der Walt, M. Brett, J. Wilson, K. J. Millman, N. Mayorov, A. R. J. Nelson, E. Jones, R. Kern, E. Larson, C. J. Carey, İ Polat, Y. Feng, E. W. Moore, J. VanderPlas, D. Laxalde, J. Perktold, R. Cimrman, I. Henriksen, E. A. Quintero, C. R. Harris, A. M. Archibald, A. H. Ribeiro, F. Pedregosa, P. van Mulbregt, and SciPy 1.0 Contributors. SciPy 1.0: Fundamental Algorithms for Scientific Computing in Python. *Nature Methods*, 17:261–272, 2020.

[77] J. D. Hunter. Matplotlib: A 2D graphics environment. *Computing in Science & Engineering*, 9:90–95, 2007.

[78] R. Kishony and S. Leibler. Environmental Stresses Can Alleviate the Average Deleterious Effect of Mutations. *J Biol*, 2:14, 2003.

[79] F. S. Midani, J. Collins, and R. A. Britton. AMiGA: Software for automated analysis of microbial growth assays. *mSystems*, 6:e00508–21, 2021.

[80] K. P. Burnham and D. R. Anderson. *Model Selection and Multimodal Inference: A Practical Information-Theoretic Approach*. Springer-Verlag, New York, 2nd edition, 2002.

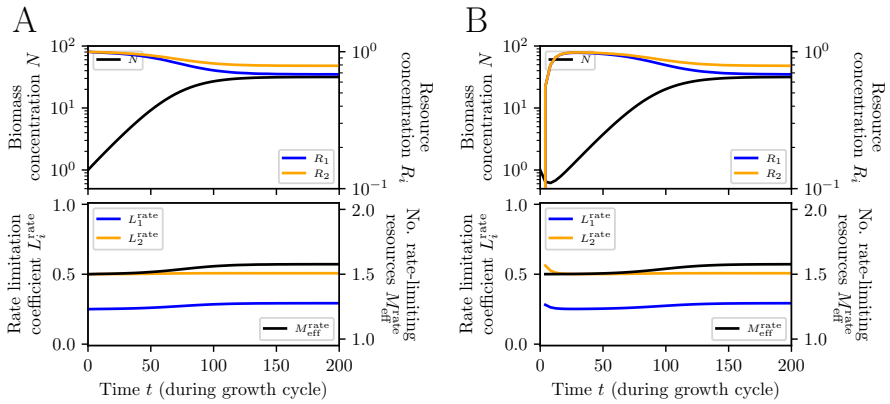

FIG. S1. **Growth and limitation dynamics in continuous (chemostat) cultures.** (A) Simulation of the system shown in Fig. 1C,D but in a chemostat regime, where the resources are supplied at constant rates and the whole system is diluted at a constant rate. The top panel shows the dynamics of biomass (black line) and resource (blue and orange) concentrations over time. The bottom panel shows the rate limitation coefficients L_i^{rate} and the number of rate-limiting resources $M_{\text{eff}}^{\text{rate}}$ over the same time range. Here the initial condition is such that the resource concentrations in the culture start at equilibrium with the supply concentrations, which the biomass growth then draws down to the steady state (see resource dynamics for the same case in Fig. S8A). (B) Same as (A) but starting with zero resource concentration in the culture (see resource dynamics in Fig. S8B).

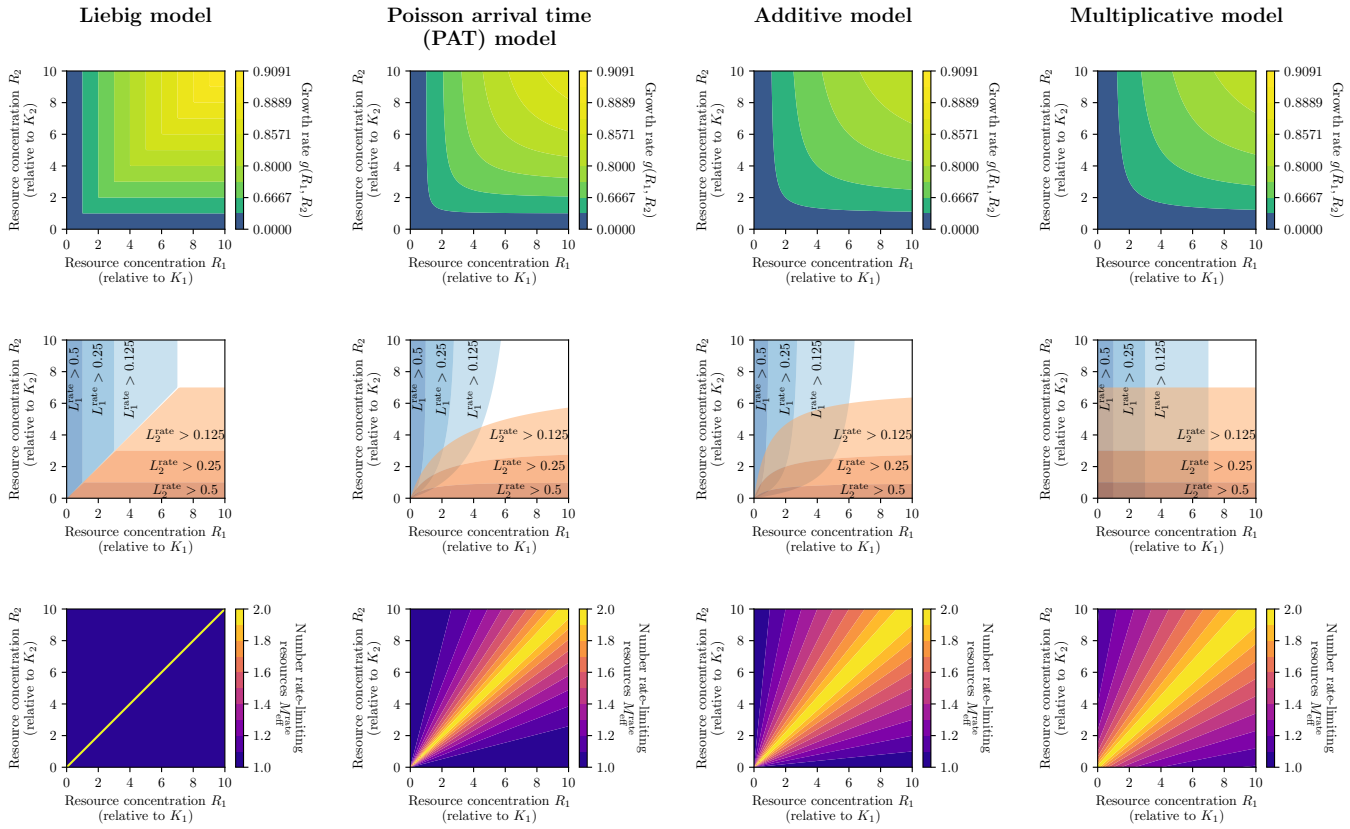

FIG. S2. **Summary of growth rate models and their limitation properties.** Each column corresponds to a different model of how growth rate depends on resource concentrations, as defined in Methods and Supplementary Information Sec. S4. First row: For each growth rate model in a different column, we show the growth rates $g(R_1, R_2)$ as functions of resource concentrations R_1 and R_2. Second row: Rate limitation coefficients for resource 1 (L_1^{rate}, blue contours) and for resource 2 (L_2^{rate}, orange contours) as functions of resource concentrations (compare to schematic in Fig. 1B). Third row: Number of rate-limiting resources $M_{\text{eff}}^{\text{rate}}$ (Eq. 3) as functions of resource concentrations. All resource concentrations R_i are scaled relative to their corresponding half-saturation concentrations K_i.

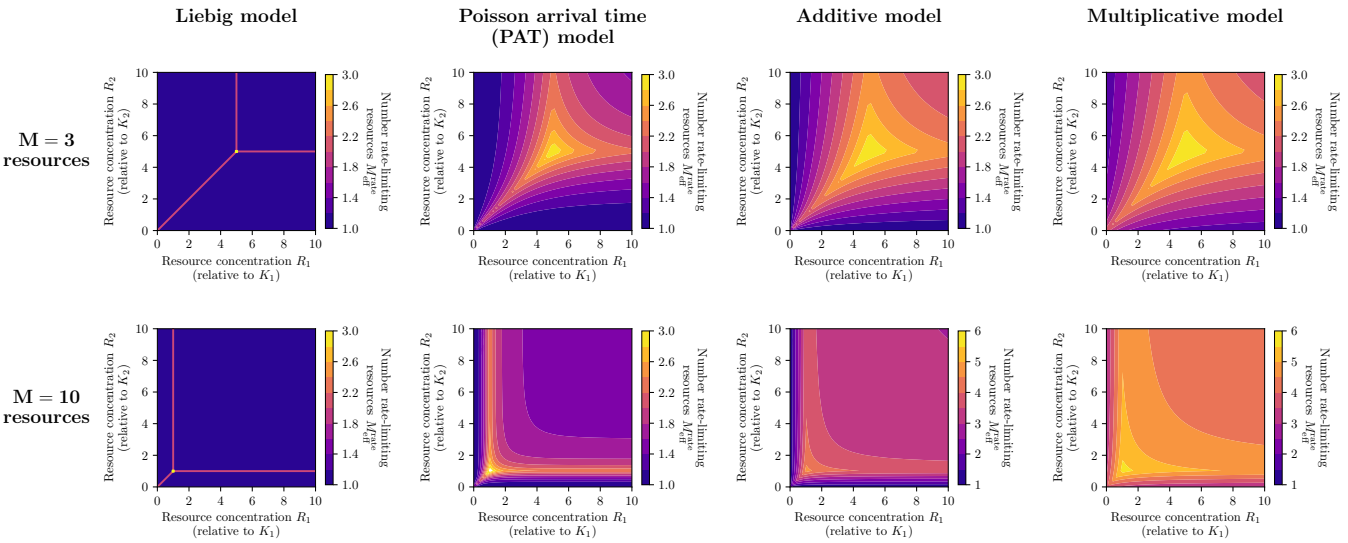

FIG. S3. **Growth rate colimitation with more than two resources.** Each column corresponds to a different model of how growth rate depends on resource concentrations, as defined in Methods and Supplementary Information Sec. S4. First row: Number of rate-limiting resources $M_{\text{eff}}^{\text{rate}}$ (Eq. 3) as functions of resource concentrations R_1 and R_2. Here there are $M = 3$ total resources, with the third resource being held fixed at $R_3/K_3 = 5$, in contrast to Fig. S2 which has similar plots but for only $M = 2$ total resources. The point at which maximum colimitation occurs ($M_{\text{eff}}^{\text{rate}} = 3$) is therefore set by the concentration of this third resource (i.e., where $R_1/K_1 = R_2/K_2 = R_3/K_3$). Second row: Same as the first row but for $M = 10$ total resources, where the additional resources are fixed at $\{R_i/K_i\} = \{5, 1, 2, 3, 4, 5, 6, 7\}$ for $i = 3, 4, \ldots, 10$. The point at which maximum colimitation occurs is set approximately by the most limiting fixed resource (resource 4 with $R_4/K_4 = 1$).

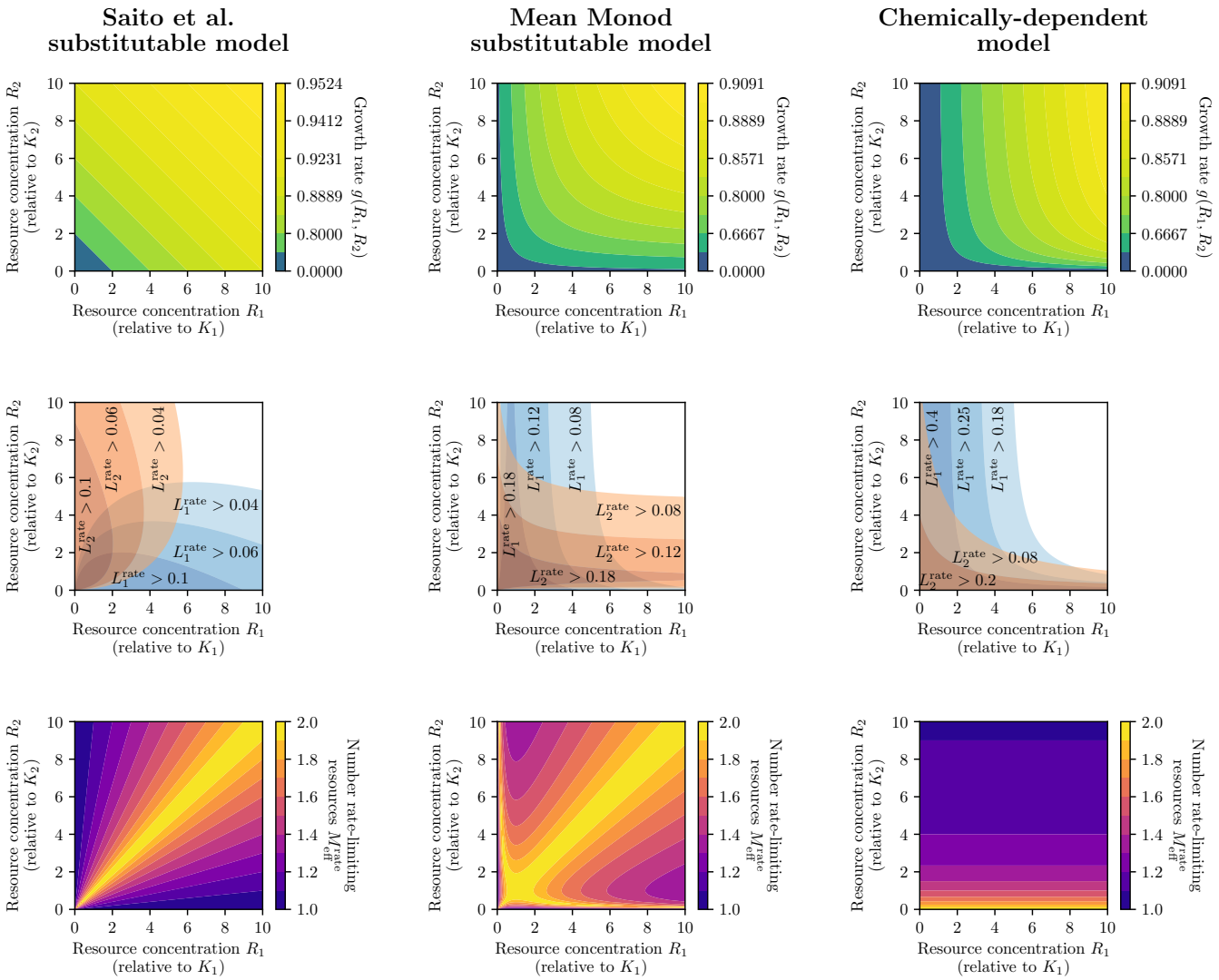

FIG. S4. **Summary of growth rate models and their limitation properties for substitutable and chemically-dependent resources.** Same as Fig. S2 but for the Saito et al. model [18] of substitutable resources (first column), the mean Monod model of substitutable resources (second column), and the model of chemically-dependent resources [18] (third column); see Supplementary Information Secs. S5 and S6 for definitions.

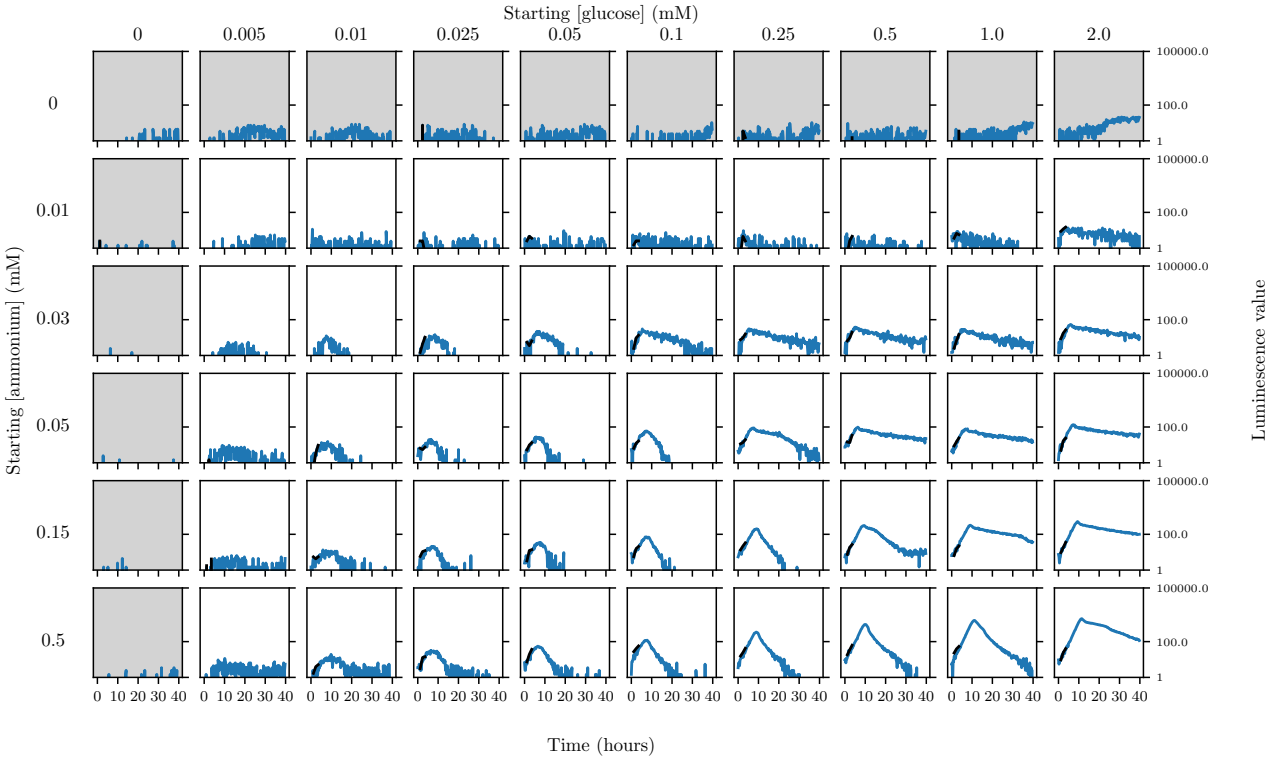

FIG. S5. **Scan of luminescence growth curves across glucose and ammonium concentrations.** Growth curves of luminescent *E. coli* sp. MG1655 pCS-λ [78] with each well having a different starting concentration of glucose and ammonium. The observed maximum growth rates, fitted from the data, are overlayed in black lines. gray shading indicates wells where the concentration of either glucose and/or ammonium was 0 μM.

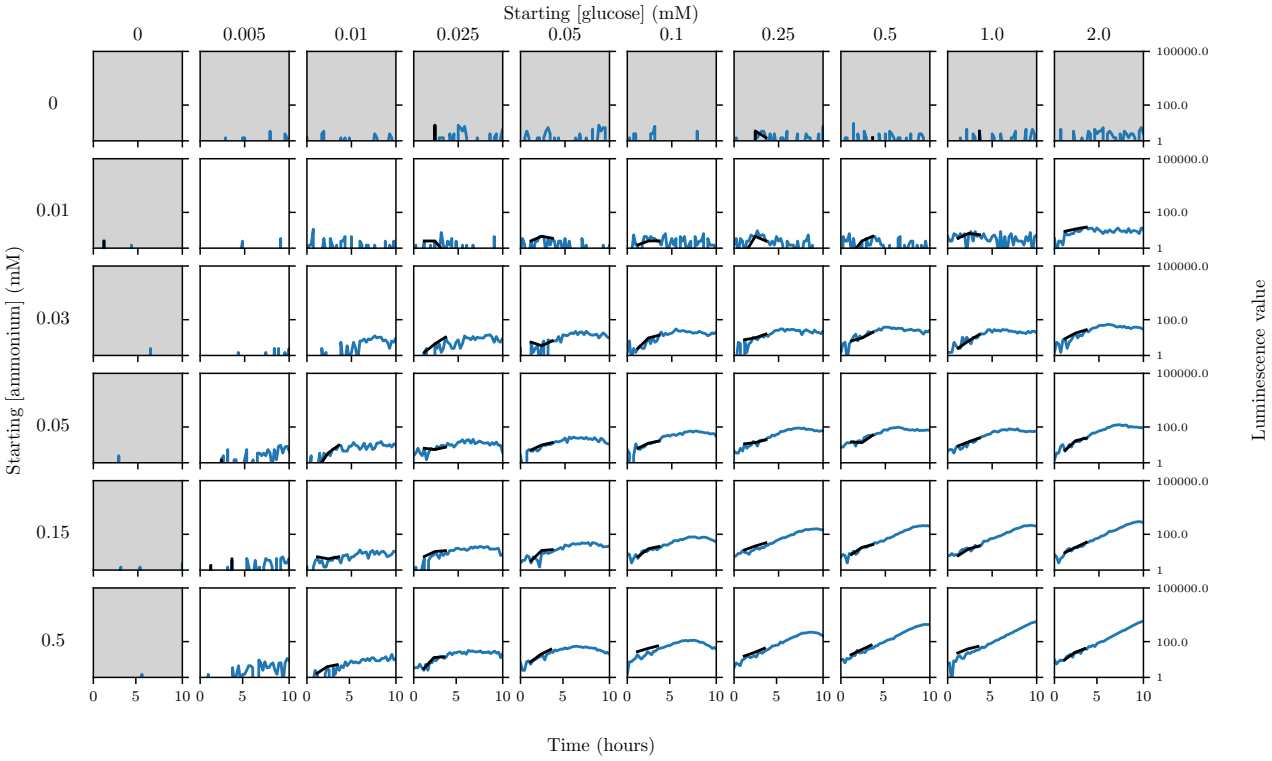

FIG. S6. **Zoomed in view of luminescence growth curves across glucose and ammonium concentrations.** Same as Fig. S5 but zoomed into the first 10 hours.

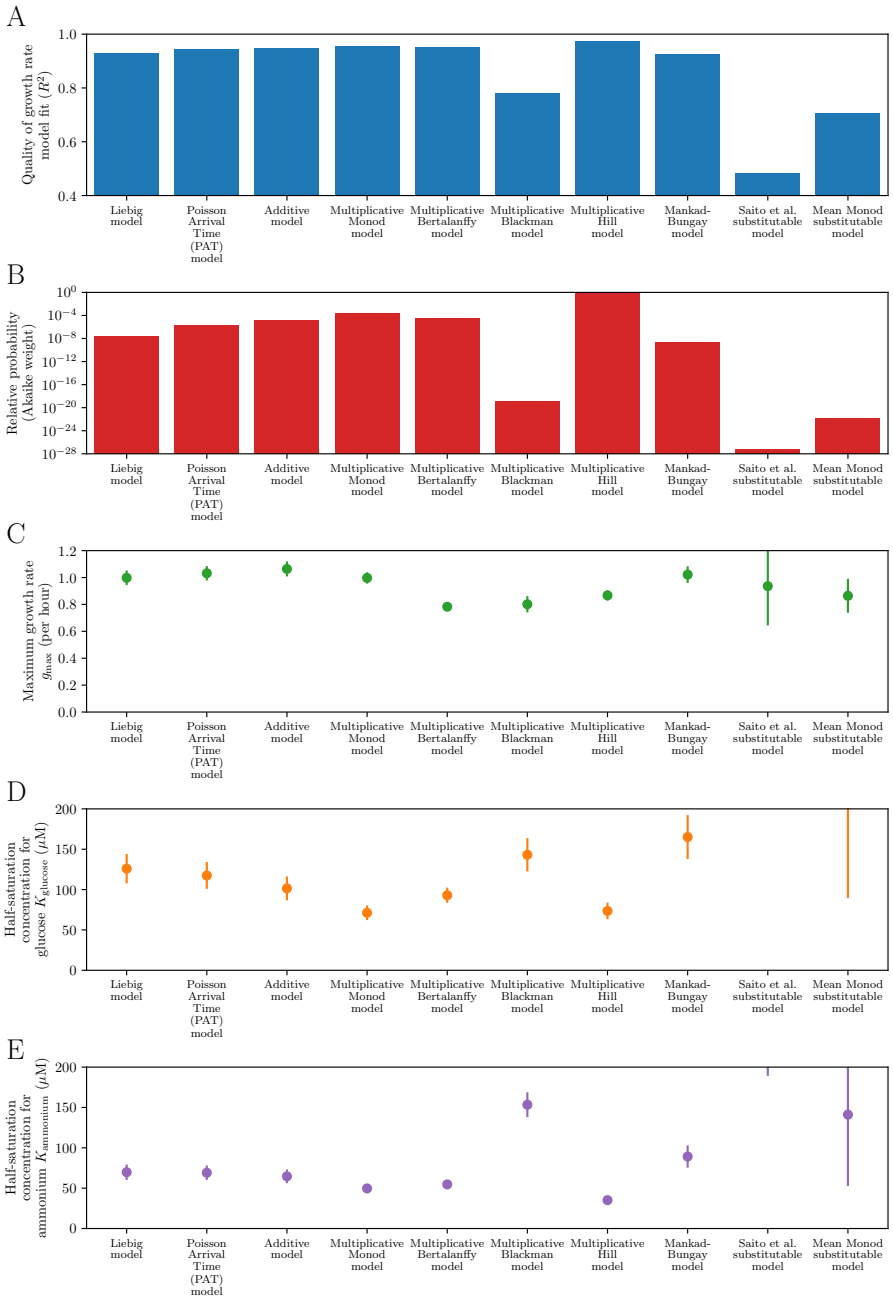

FIG. S7. **Statistics for fitting different growth rate models to experimental data.** We fit several growth rate models (Methods, Supplementary Information Sec. S4) to the population growth rate of *E. coli* as a function of glucose and ammonium concentrations (Figs. 2A, S5, and S6). (A) Quality of fit R^2 for each model. (B) Relative probability of each model fit using its Akaike weight. (C) Value of the maximum growth rate $g_{\max}$ for each fit, with estimated standard deviations shown as vertical bars. (D) Same as (C) but for the fitted half-saturation concentration K_{glucose} for glucose. (D) Same as (C) but for the fitted half-saturation concentration K_{ammonium} for ammonium.

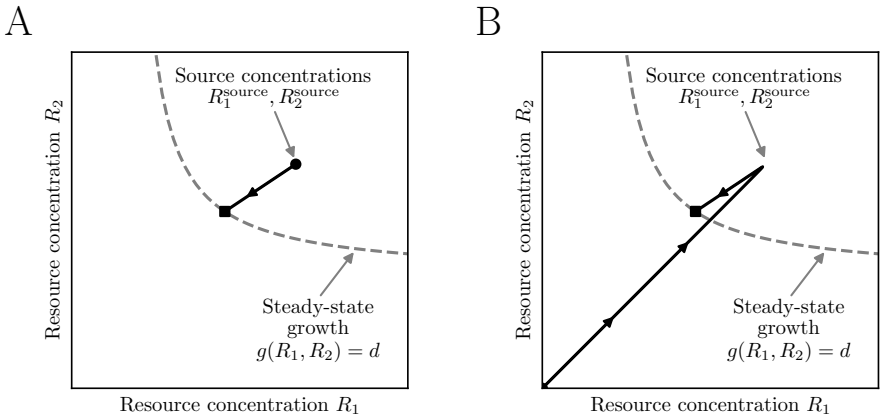

FIG. S8. **Resource dynamics for continuous (chemostat) cultures.** (A) Dynamics of resource concentrations for the same simulation in Fig. S1A. This simulation begins with resources in equilibrium with their source concentrations (black dot), but as the biomass grows, they draw down along a trajectory (black line with arrow) with slope set by their stoichiometry (Supplementary Information Secs. S2 and S8) until they intersect the gray curve (black square) where biomass growth rate equals dilution rate. (B) Same as (A) but for simulation in Fig. S1B, which is the same model but with resources starting at zero concentration in the culture. In this case, the resources initially draw up to reach their source concentrations, but then draw down to the steady state with biomass growth as in (A).

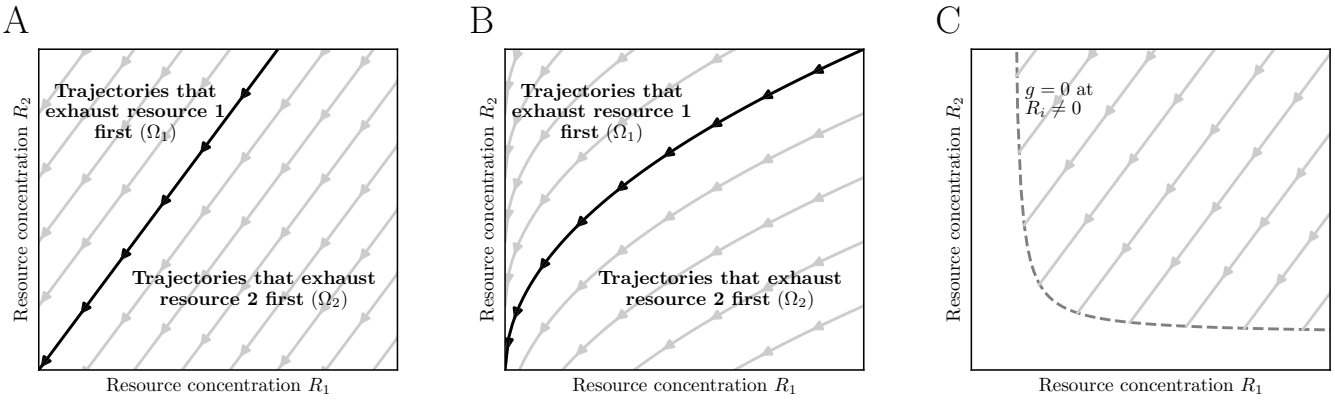

FIG. S9. **Different qualitative regimes of resource depletion trajectories.** (A) If resources are consumed with constant stoichiometry, then their concentrations deplete along straight lines (Supplementary Information Sec. S8). The regions in which the first depleted resource is resource 1 or resource 2 are shown as Ω_1 and Ω_2. (B) Same as (A) but for resources consumed with variable stoichiometry, which causes their depletion trajectories to curve (Supplementary Information Sec. S8). (C) Same as (A) for where resource depletion stops at some nonzero combination of concentrations (dashed gray line), e.g., when growth rate reaches zero.

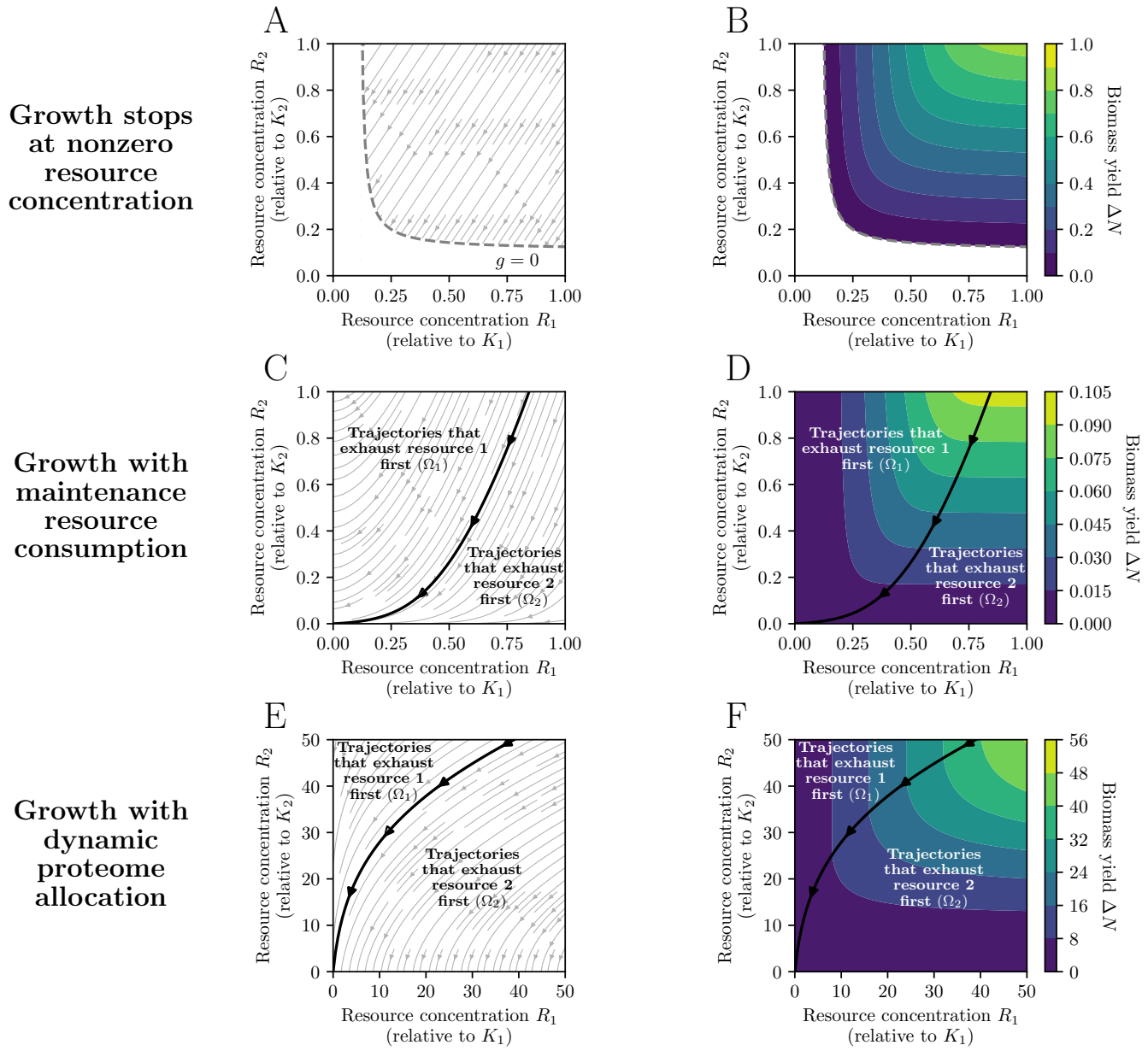

FIG. S10. **Yield limitation in different mechanistic models.** (A) Model of resource consumption in which growth stops at nonzero concentrations of resources (Supplementary Information Sec. S8). These concentrations (Zero Net Growth Isocline, ZNGI) are shown as the dashed gray line in the space of concentrations for resources 1 and 2. Gray stream lines show trajectories of resource depletion with constant stoichiometry. (B) For the model in (A), we calculate the total biomass yield ΔN after one batch growth cycle for all possible initial resource concentrations. (C) Model of resource consumption in which biomass consumes resources for maintenance as well as growth (Supplementary Information Sec. S9). This causes stoichiometry to vary with resource concentration, and so depletion trajectories are curved. (D) Same as (B) but for the maintenance model in (C). The regions in which the first depleted resource is resource 1 or resource 2 are shown as Ω_1 and Ω_2. (E) Model of resource consumption in which stoichiometry varies with growth rate according to changes in proteome allocation (Supplementary Information Sec. S10). This causes stoichiometry to vary with resource concentration, and so depletion trajectories are curved. (F) Same as (D) but for the dynamic allocation model in (E).

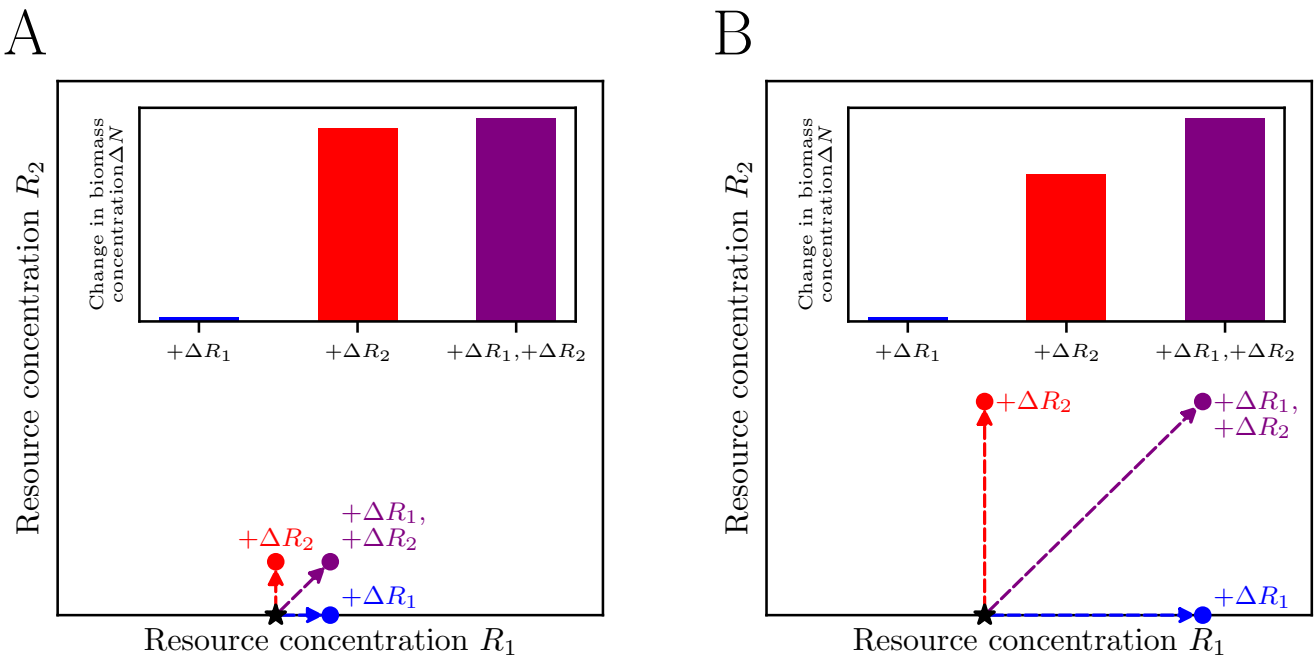

FIG. S11. **Resource supplementation outcomes with non-Liebig yield limitation.** Same as Fig. 4B,C but where biomass yield has non-Liebig dependence on resource concentrations (generalized-mean model with $q = -1$; Eq. 7, Methods, and Supplementary Information Sec. S12).

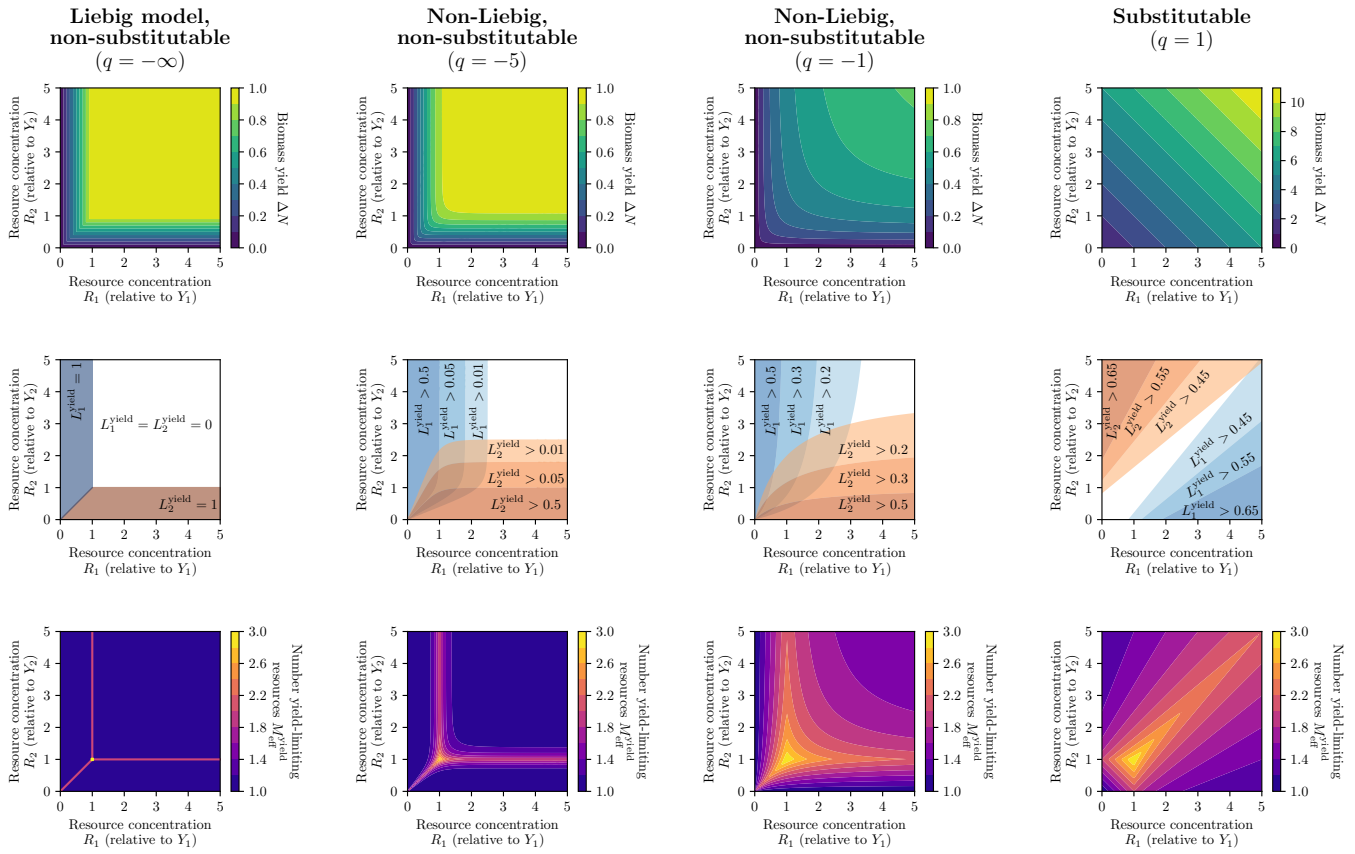

FIG. S12. **Generalized-mean model of yield limitation.** Each column corresponds to the generalized-mean model of biomass yield (Eq. 7 and Supplementary Information Sec. S12) with a different value of the resource interaction parameter q. The limit of $q = -\infty$ is equivalent to the Liebig model of biomass (Eq. 6); $q < 0$ describes non-substitutable resources, while $q > 0$ describes substitutable resources. First row: Total biomass yield over a batch growth cycle as a function of initial supplied resource concentrations R_1 and R_2. Second row: Yield limitation coefficients for resource 1 (L_1^{yield}, blue contours) and for resource 2 (L_2^{yield}, orange contours) as functions of resource concentrations. Third row: Number of yield-limiting resources $M_{\text{eff}}^{\text{yield}}$ (Eq. 5) as functions of resource concentrations. All resource concentrations R_i are scaled relative to their corresponding yields Y_i. We also assume the next most yield-limiting resource contributes biomass $R_3 Y_3 = 1$ (Supplementary Information Sec. S12).

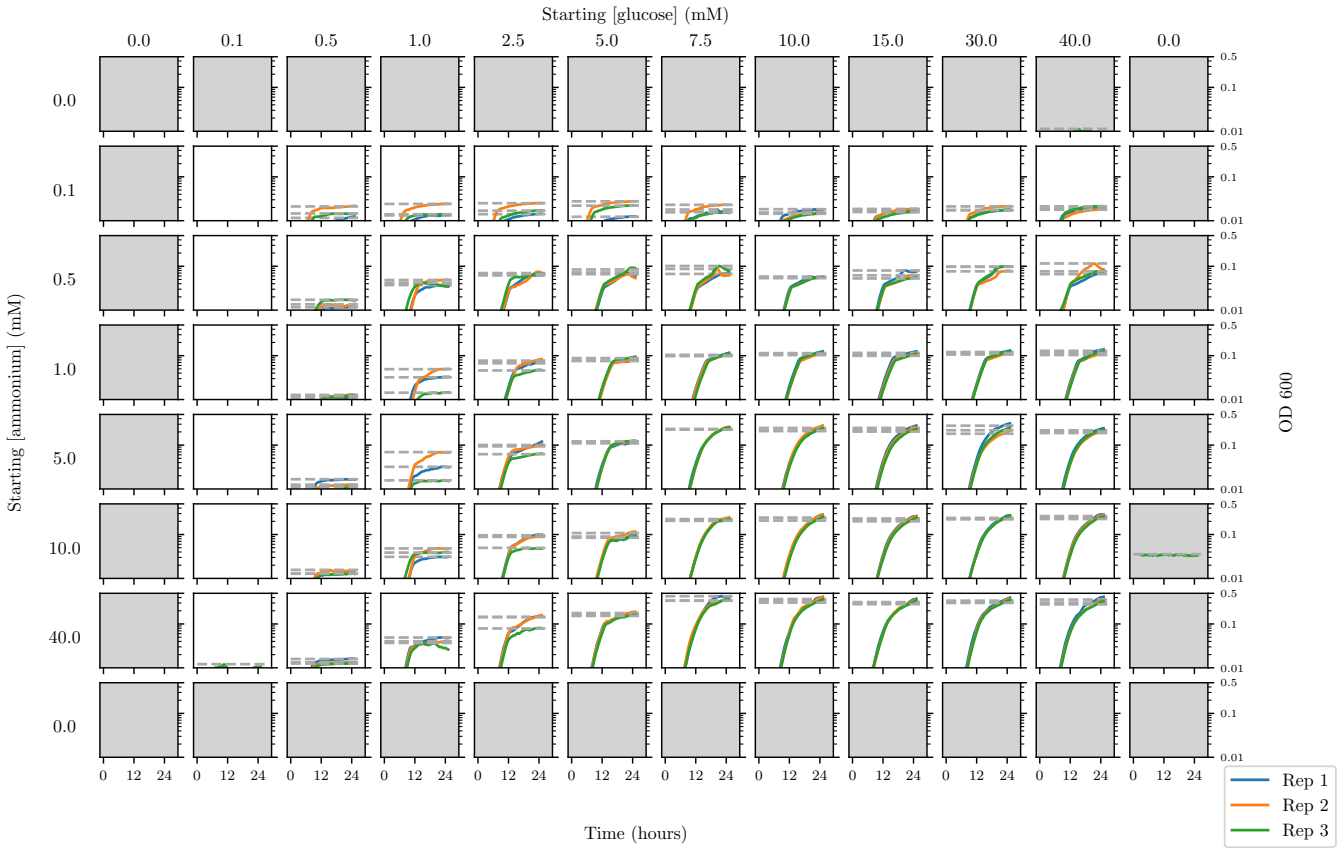

FIG. S13. **Scan of optical density growth curves across glucose and ammonium concentrations.** Growth curves of optical density at 600 nm for *E. coli* sp. MG1655 pCS-λ [78] with each well having a different starting concentration of glucose and ammonium. Triplicate growth curves are shown as colored lines; the observed biomass yields, fitted from the data, are overlayed in gray dotted lines.

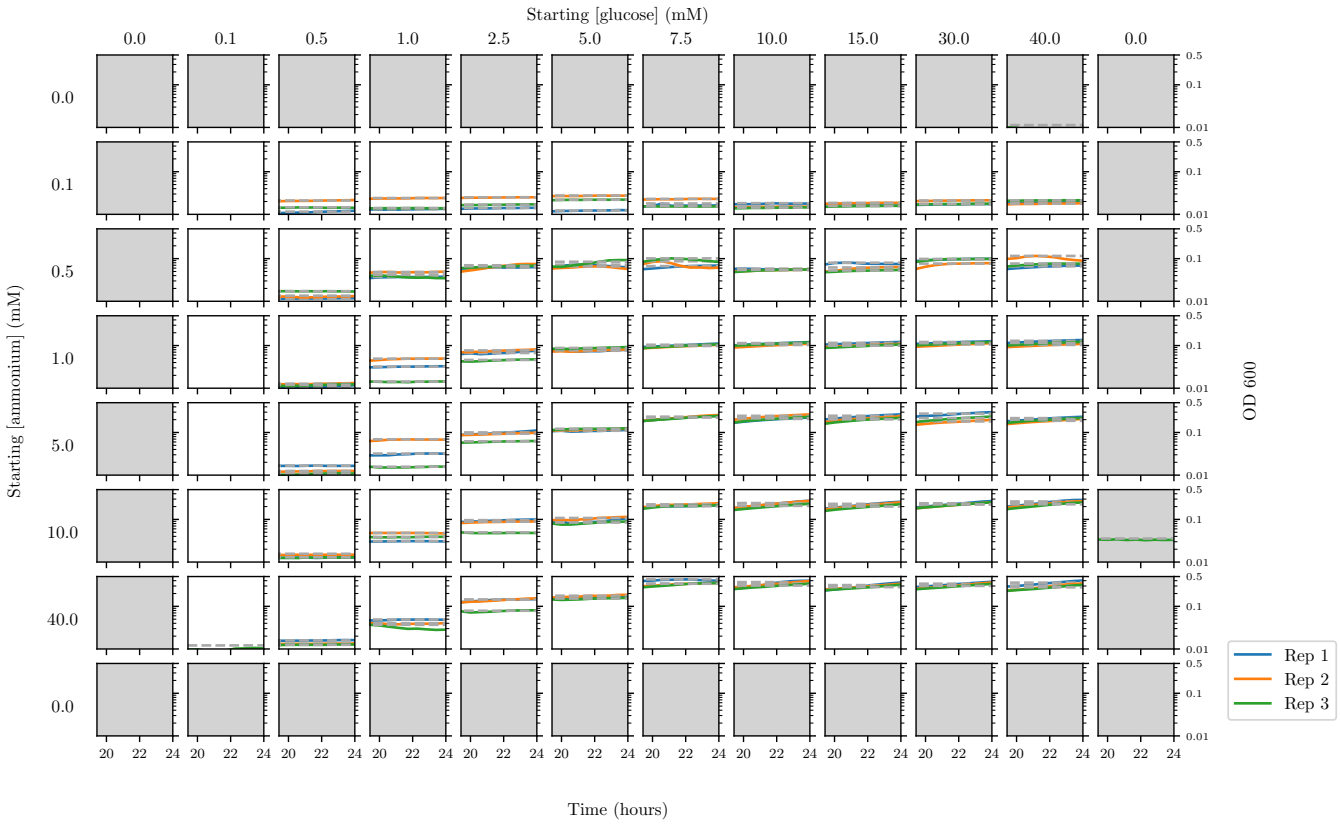

FIG. S14. **Zoomed in view of optical density growth curves across glucose and ammonium concentrations.** Same as Fig. S13 but zoomed into the time window between 20 and 24 hours where biomass yield is maximum.

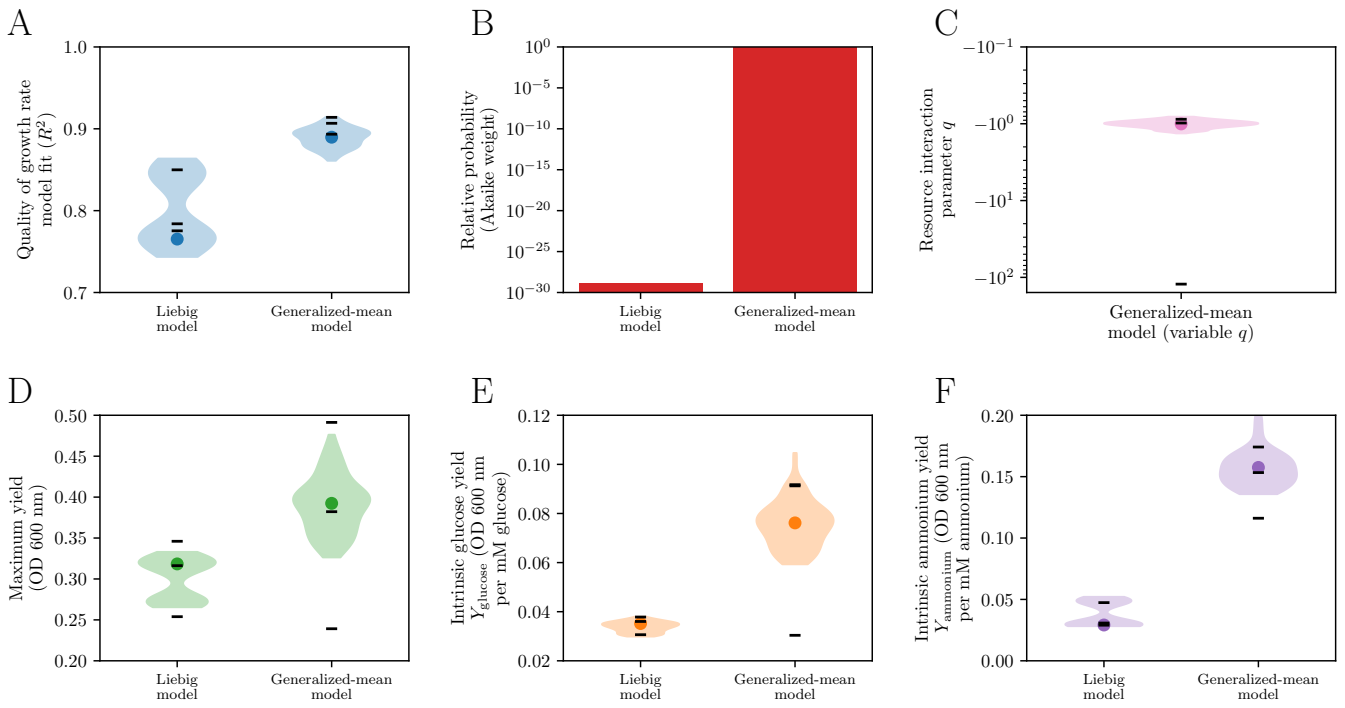

FIG. S15. **Statistics for fitting different yield models to experimental data.** We fit the Liebig model (Eq. 6) and the generalized-mean model (Eq. 7) to the biomass yield of *E. coli* as a function of glucose and ammonium concentrations (Figs. 5A, S13, and S14). (A) Quality of fit R^2 for each model. The dots represent the fit using all three experimental replicates, and the black horizontal bars represent fits for each replicate separately. The violins represent fits for 100 simulated data sets bootstrapped from the experimental replicates (Methods). (B) Relative probability of each model fit using its Akaike weight. (C) Same as (A) but showing fitted values of the resource interaction parameter q (only valid for the generalized-mean model). (D) Same as (A) but showing fitted values of the maximum yield. (E) Same as (A) but showing fitted values of the intrinsic glucose yield Y_{glucose}. (F) Same as (A) but showing fitted values of the intrinsic ammonium yield Y_{ammonium}.